NASA TECHNICAL NOTE

NASA TN D-7030

BOUNDARY LAYER MEASUREMENTS IN AN ACCELERATED FLOW WITH AND WITHOUT HEAT TRANSFER

by Howard L. Wesoky and Charlene May

Lewis Research Center
Cleveland, Ohio 44135

NATIONAL AERONAUTICS AND SPACE ADMINISTRATION • WASHINGTON, D. C. • JANUARY 1971

1. Report No.	2. Government Accession No.	3. Recipient's Catalog No.
NASA TN D-7030		

4. Title and Subtitle: BOUNDARY LAYER MEASUREMENTS IN AN ACCELERATED FLOW WITH AND WITHOUT HEAT TRANSFER

5. Report Date: January 1971

6. Performing Organization Code:

7. Author(s): Howard L. Wesoky and Charlene May

8. Performing Organization Report No.: E-5674

9. Performing Organization Name and Address:
Lewis Research Center
National Aeronautics and Space Administration
Cleveland, Ohio 44135

10. Work Unit No.: 129-01

11. Contract or Grant No.:

12. Sponsoring Agency Name and Address:
National Aeronautics and Space Administration
Washington, D.C. 20546

13. Type of Report and Period Covered: Technical Note

14. Sponsoring Agency Code:

15. Supplementary Notes:

16. Abstract

Experimental velocity and temperature profiles for the adiabatic and cooled boundary layers on a cylindrical body in an accelerated flow have been presented for a range of free-stream Mach numbers from 0.21 to 0.97. High acceleration caused thinning of the momentum boundary layer, but cooling the same boundary layer increased the velocity and momentum thicknesses over the corresponding adiabatic values. Growth of the thermal boundary layer far outside the momentum boundary layer was also caused by high acceleration. Use of a standard mixing length hypothesis in integration of the boundary layer equations yielded fairly accurate predictions of the boundary-layer thickness.

17. Key Words (Suggested by Author(s))	18. Distribution Statement
Turbulent boundary layer Acceleration effects	Unclassified - unlimited

19. Security Classif. (of this report)	20. Security Classif. (of this page)	21. No. of Pages	22. Price*
Unclassified	Unclassified	46	$3.00

*For sale by the National Technical Information Service, Springfield, Virginia 22151

BOUNDARY LAYER MEASUREMENTS IN AN ACCELERATED FLOW WITH AND WITHOUT HEAT TRANSFER

by Howard L. Wesoky and Charlene May

Lewis Research Center

SUMMARY

Experimental velocity and temperature profiles for the adiabatic and cooled boundary layers on a cylindrical body in an accelerated flow have been presented for a range of free-stream Mach numbers from 0.21 to 0.97. A strong favorable pressure gradient caused the measured wake component of the velocity profiles to disappear. The momentum layer was thinned by acceleration, but cooling the same boundary layer caused an increase in velocity and momentum thicknesses over their corresponding adiabatic values. High acceleration caused the thermal boundary layer to become thicker than the momentum boundary layer. A noticeable wake component of the temperature profile existed at each station. Increased resistance to heat transfer would undoubtedly result from the growth of the thermal boundary layer into a region of low eddy conductivity.

The measurements were compared to results of a numerical integration of the boundary-layer equations using a standard mixing-length model for the turbulent viscosity. Results of the calculations were strongly dependent on the initial condition where the pressure gradient was small, and almost independent of the initial conditions where the pressure gradient was large. Predictions of momentum, displacement and energy thicknesses had an average error of 8 percent in regions of low acceleration, and 29 percent in regions of high acceleration.

INTRODUCTION

Previous measurements in highly accelerated turbulent flows have indicated a reduction in heat-transfer level below that considered typical of turbulent boundary layers (refs. 1 to 5). Although the reason for this has generally been attributed to laminarization of the boundary layer, or transition towards a more laminar-like flow, few boundary-layer measurements have been made under strong favorable pressure gradient

conditions (refs. 1, 2, 4, and 6). In particular, very little information exists about the region where the pressure gradient and corresponding reduction in heat transfer are the greatest.

Experimental data reported here are from a study of the turbulent boundary layer in an axisymmetric flow with a cooled wall. Mean velocity and temperature boundary layer profiles were measured on a constant diameter centerbody over which heated air was highly accelerated by a nozzle. Heat transfer was provided by flowing cold nitrogen gas through the centerbody. An attempt to measure the heat transfer using a transient method based on the heat storage capacity of the centerbody wall was not successful, but is discussed in terms of the difficulties encountered. The boundary-layer measurements were made with and without heat transfer, providing an interesting examination of the combined effects of cooling and acceleration. Velocity and temperature profile data were obtained at five stations having free-stream Mach numbers between 0.21 and 0.97 with the use of miniature pitot tubes and probes which combined pitot tubes with thermocouples for total temperature measurement.

The scope of the present work is to present results of the measurements and to compare these with a solution to the boundary layer equations which uses a standard mixing length model for the eddy diffusivity (ref. 7). Also the results are discussed in terms of previous similar studies and the suggested acceleration criteria for reduction of the turbulent heat-transfer level.

SYMBOLS

b	centerbody wall thickness
C	pitot tube recovery factor
C_f	friction coefficient
C_p	specific heat
h	heat-transfer coefficient
K	acceleration parameter
k	thermal conductivity
M	local Mach number
M_e	free-stream Mach number
P	static pressure
P_o	plenum pressure
P_T	total pressure

P'_T	measured recovery pressure
P'_{Te}	measured free-stream recovery pressure
Q_h	convective heat flux
Q_k	conductive heat flux
Q_s	rate of heat storage
R	centerbody radius
St	Stanton number, $h/\rho_e C_p u_e$
T_{aw}	adiabatic wall temperature
T_o	plenum temperature
T_R	measured temperature
T_T	total temperature
T_w	wall temperature
T^+	dimensionless temperature (see eq. (10))
t	time
u	velocity
u_e	free-stream velocity
u_τ	shear velocity (see eq. (12))
u^+	dimensionless velocity (see eq. (9))
x	axial distance measured from upstream centerbody thermocouple
y	radial distance measured from centerbody
y^+	dimensionless radial distance (see eq. (8))
z	axial distance measured from nozzle throat
Δ	boundary-layer temperature thickness (distance from wall where $(T_T - T_w)/(T_o - T_w) = 0.99$)
δ	boundary-layer velocity thickness (distance from wall where $u/u_e = 0.99$)
δ^*	boundary-layer displacement thickness
η	total-temperature recovery factor
θ	boundary-layer momentum thickness
ν	kinematic viscosity
ρ	local density

ρ_e free-stream density

φ boundary-layer energy thickness

APPARATUS

Airflow System

A schematic drawing of the test facility is shown in figure 1. The airflow system and test section nozzle geometry were the same as reported in reference 6. A high-pressure dry air supply was expanded to near atmospheric pressure in the plenum, which received the air through a large perforated pipe, reducing the flow velocity and causing thorough mixing. The upstream fiberglass blanket filter, being open to the atmosphere, kept the wood plenum from being damaged by over pressurization, and allowed a small flow to the surroundings when the test section nozzle flow was choked. Solid particles in the air were removed by the downstream filter, and, after flowing through the bell mouth inlet and test section, the air was exhausted into a 2 psia (13.8 kN/m^2) vacuum system. Flow rate of the air was approximately 5.1 pounds per second (2.3 kg/sec).

Upstream of the plenum was a steam heat exchanger (not used in ref. 6) which heated the air to approximately 645° R (358 K). The desired temperature was set before each test and was controlled during the test by a pneumatic control system which varied the steam flow rate according to a plenum temperature measurement. Plenum pressure and temperature were constantly monitored by a pitot tube and thermocouple ahead of the bellmouth entrance to the test section. Both the plenum pressure and temperature varied slightly between tests because of changes in the atmospheric condition and steam system pressure and temperature, but variations during an individual test were insignificant.

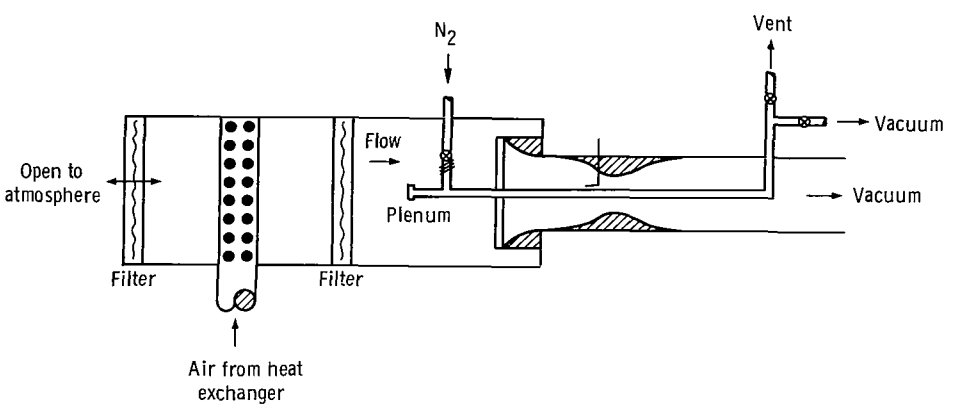

Figure 1. - Boundary-layer and heat-transfer facility. Air flow rate, 5 pounds per second (2.25 kg/sec); plenum pressure, 1 atmosphere; plenum temperature, 645° R (358 K); coolant flow rate, 0.1 pound per second at 55 psia (0.045 kg/sec at 379 kN/m^2).

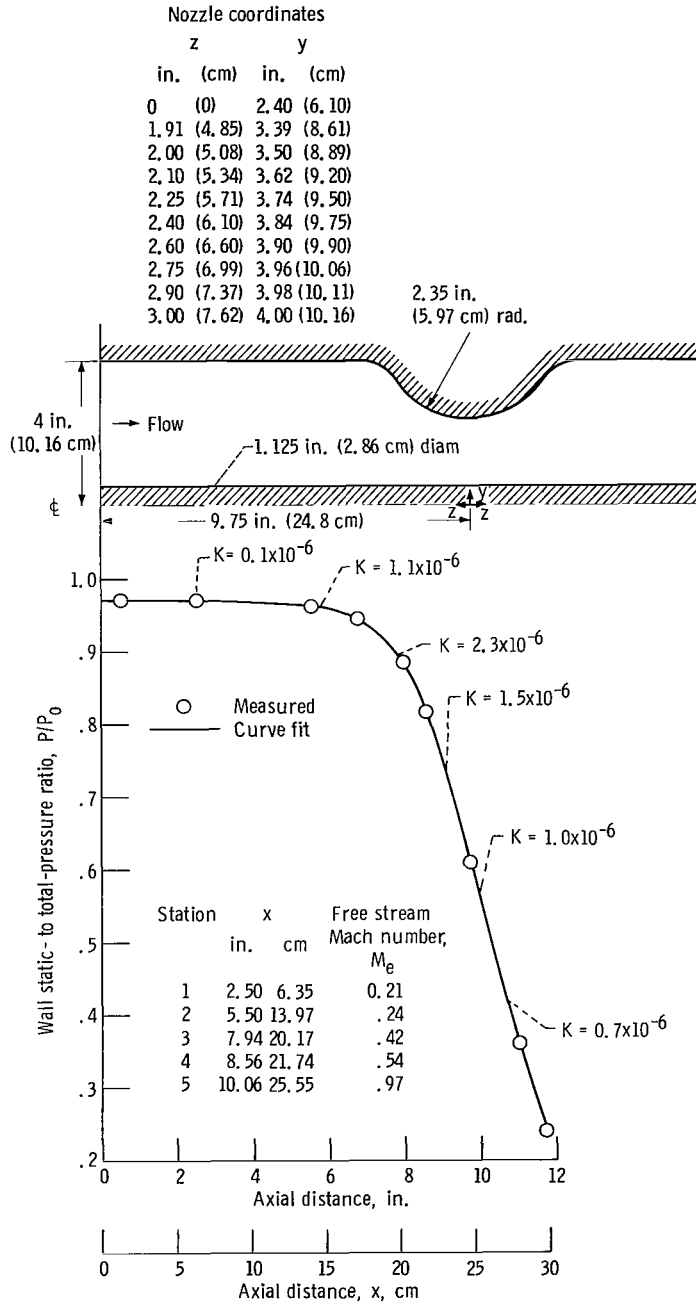

Figure 2. - Test section geometry, pressure, and acceleration distributions.

Test Section Nozzle and Inlet

The axisymmetric test section, shown schematically in figure 2, consisted of a constant area inlet connected to a nozzle which had the same geometry as the high gradient nozzle referred to in reference 6. A large bellmouth, shown in figure 1, was attached upstream (x = 0 in fig. 2) to give a uniform flow at the test section entrance. The bellmouth, inlet, and nozzle were constructed from mahogany and given a fine lacquer finish. A 10 inch (25.4 cm) diameter steel pipe encased the inlet and nozzle, which were attached to only the upstream end of the pipe to allow for any small shrinkage due to changes in moisture content of the wood. The boundary layer on the centerbody was investigated with instruments mounted to traversing devices on the test section inlet and nozzle wall. Five boundary layer measuring stations, whose axial positions are listed in figure 2, were used in the experiment. The first two stations were in the constant area inlet, the others in the nozzle. Mach numbers, listed with the axial positions, correspond to static pressures measured on the centerbody. The distribution of static to total pressure ratio on the centerbody is shown also in figure 2 with a flow acceleration parameter discussed later.

Coolant Flow System

To provide heat transfer, cold nitrogen gas flowed through the test section centerbody described later and was warmed by the air flowing over the centerbody. The source of the coolant gas was a liquid-nitrogen dewar pressurized to approximately 55 psia (379 kN/m^2). This pressure was attained by boiling the liquid nitrogen in a radiator, with the resulting gas used to control the pressure above the liquid and also to flow through the test section as a coolant. The pressure was controlled by varying the flow rate through the radiator with a spring loaded valve. Any oscillations in the pressure were damped by a large tank in the nitrogen system upstream of the test section. The flow rate through the test section was controlled by a pneumatic system which operated a valve downstream of the test section centerbody. This controller was sensitive to a centerbody wall temperature, measured with a thermocouple. The amount of cooling was restricted by the dew point of the air, about 440° R (244 K). Frost formation on the centerbody was avoided by adjusting the set point of the controller so that the centerbody temperature was never below 450° R (250 K). Absence of frost was confirmed by observation of the test section through a window in the plenum. The nitrogen flow rate was not measured, but observation of the liquid level in the dewar yielded an estimate of less than 0.1 pound per second (0.045 kg/sec). During the steady-state portion of a test the nitrogen gas was exhausted to the atmosphere through the vent indicated in figure 1.

During a heat-transfer measurement, the valve upstream of the test section (see fig. 1) and the flow-control valve downstream of the test section were closed, and a valve connecting the centerbody to the vacuum system discussed previously was opened. In this way, the nitrogen could be quickly evacuated from the centerbody. This was necessary for the heat-transfer measurement discussed in the Procedure and Data Reduction section.

Centerbody

A schematic drawing of the test section centerbody is shown in figure 1. Its length between the vertical inlet and outlet sections of the nitrogen coolant system was 33.4 inches (84.8 cm). The part of the centerbody within the inlet and nozzle portions of the test section was constructed from 1.125-inch (2.86-cm) diameter copper tube with 0.048-inch (0.122-cm) wall thickness. This copper tube was soldered at both ends to 1-inch (2.54-cm) diameter stainless-steel tubes with 0.065-inch (0.165-cm) wall thickness. The step in the centerbody diameter occurred in the bellmouth, 7 inches (17.8 cm) upstream of the first boundary-layer measuring station indicated in figure 2. At the upstream end, the centerbody was supported by three struts connected to the bellmouth, which restrained movement only in the radial direction, and at the downstream end it was supported by one strut and the tubing in the coolant vent line, which were rigidly connected to the test section wall. Supports at both ends were adjustable so that the centerbody could be accurately positioned in the axisymmetric test section. The upstream end was connected to the nitrogen coolant system through a bellows which allowed the centerbody to move axially when its length was altered by temperature gradients, and also to be unaffected by similar changes in length of the upstream coolant system tubing. Since the temperature of the centerbody was only reduced about 80° R (45 K) below ambient conditions, any change in its length was minimal (approximately 0.001 to 0.003 in. (0.0025 to 0.0075 cm)).

The centerbody was instrumented with nine pressure taps and 13 thermocouples. The three thermocouples at the downstream end of the test section were disregarded in data reduction due to a nearby shock wave discovered during preliminary static-pressure measurements, which made interpretation of the data from these impossible. Small stainless-steel tubing (0.040 in. (0.102 cm) diam)) was used for the pressure tap leads and thermocouple sheaths to reduce coolant flow blockage and heat leaks. Chromel-constantan alloy thermocouples were used in all temperature measurements in this experiment. The centerbody thermocouple junctions were formed by stripping the insulation from a short length of swaged lead wire and welding the bared alloy wire to the sheath. Each thermocouple was X-rayed to make sure the junction would be within the

thickness of the copper wall in which it was to be placed. Thermocouple and pressure tap leads were connected to the copper wall of the centerbody with a low melting point silver type solder.

The instrumentation was arranged in the form of two helixes along the axis of the centerbody, each covering 180°. Location of the pressure taps is indicated in figure 2 with the static-pressure distribution, and the thermocouple positions will be indicated later when the temperature distribution is discussed. Some slack was left in each instrumentation lead to reduce stresses in the leads due to thermal expansion of the system.

From the centerbody, the instrumentation tubing was led in a bundle to junctions outside the plenum. Static pressures were measured with mercury and oil manometers referenced to the atmosphere, and the thermocouple readings were monitored with a self-balancing potentiometer. An automatic voltage digitizer was used to read the temperatures during the attempted heat transfer measurement which is discussed in appendix A.

Boundary-Layer Instrumentation

Two primary types of boundary-layer instrumentation were used in the experiment. The first was ordinary pitot tubes, the second was a combination of a pitot tube and a total temperature probe. A typical combination probe is shown in figure 3. Very small probes were, of course, necessary because of the thin boundary layers encountered. Pitot tube mouths had a maximum height, including the 0.001-inch (0.00254-cm) wall thickness, of about 0.010 inch (0.0254 cm), and the temperature probes were constructed from chromel-constantan thermocouples having 0.008 inch (0.0203 cm) sheath diameter. The stainless steel thermocouple sheaths were soldered to the side of the pitot tubes as shown in figure 3. Maximum width of this assembly was approximately 0.040 inch (0.102 cm).

Both circular and rectangular pitot mouths were used in the experiments. The inclination of the pitot tubes was necessary to insure that only the mouth contacted the centerbody. Although rectangular mouths are desirable, since these can be made smaller in general, they gave inaccurate measurements at the Mach 0.42 and 0.54 stations indicated in figure 2. Because of the inclination of the pitot tubes to the centerbody axis, the pressure recovery of the rectangular probes was not good at the boundary-layer edge at these stations where the streamlines had an opposite inclination to the centerbody axis. Round pitot mouths, with a 15° internal chamber, gave good results at these measuring stations, and the data reported here for these stations were measured with round pitot tubes only. Reference 8 indicates that accurate measurements can

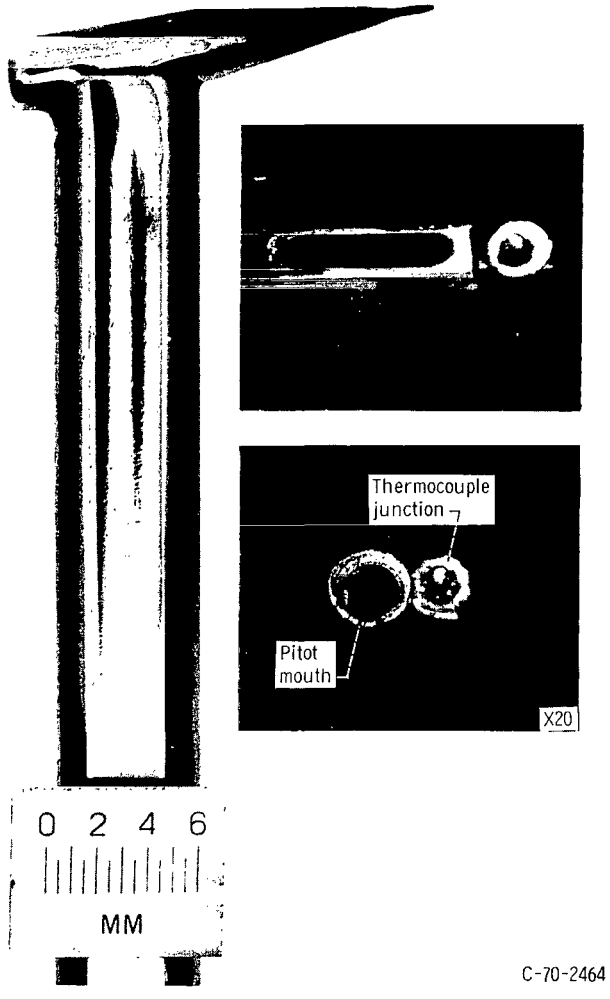

Figure 3. - Combination pitot and thermocouple boundary layer probe.

be made with this type of probe in flows inclined as much as 30^{o}, which is higher than the inclination was in this experiment. A comparison of measurements made with ordinary pitot tubes (without a thermocouple) at the $M = 0.42$ station is shown in figure 4. The round pitot mouth had a height of 0.010 inch (0.0254 cm) and the rectangular mouth was 0.007 inch (0.0178 cm) high. At the two upstream stations, both shapes of pitot tubes were used, while at the Mach 0.97 station only rectangular pitot mouths were used in order to insure that the probe height was less than 25 percent of the boundary-layer velocity thickness, as discussed in reference 6. Ordinary pitot tubes and the combination type probe were both used for the adiabatic boundary-layer measurements. Agreement between these was taken as proof of the accuracy of the combination probe for which no data were known prior to these tests. An independent calibration of the tem-

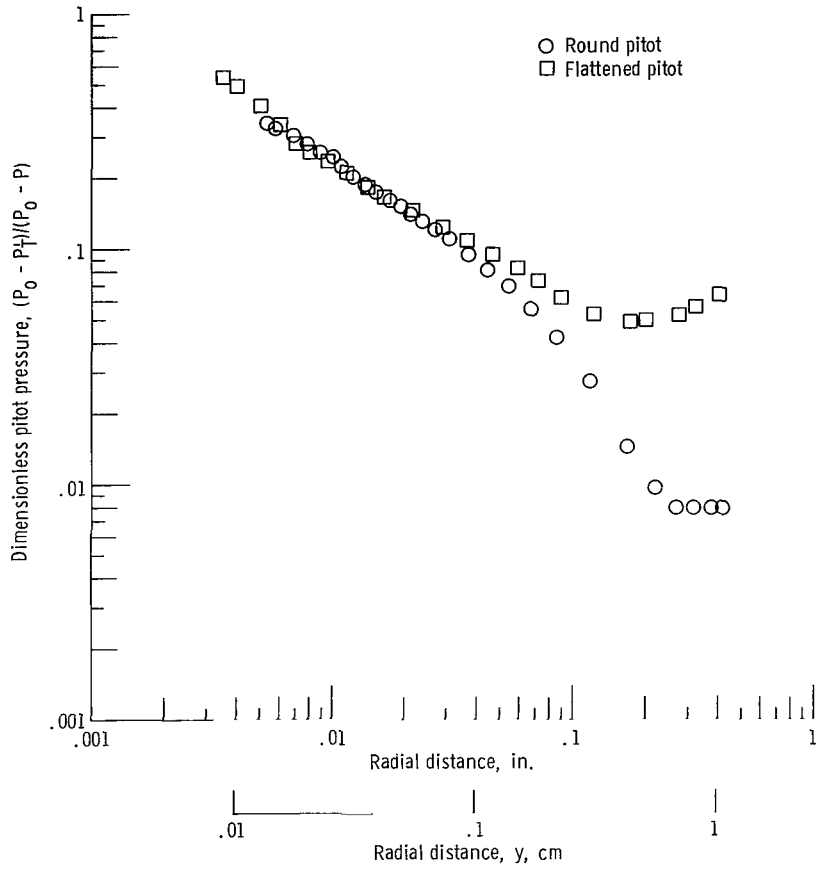

Figure 4. - Round and flattened pitot data, station number 3, $M_e = 0.42$.

perature and pressure recovery characteristics of all probes was conducted in a jet flow facility built for this purpose at the Lewis Research Center. Both pressure and temperature measurements made in the free stream of the test section used in this experiment compared favorably with the independent calibration.

The boundary-layer instrumentation was mounted in electrically driven actuators on the test section wall. Position measurement was with a dial indicator, integral to the actuator mechanism, and was accurate to 0.1 percent of the full actuator travel. Actuators having 0.5-inch (1.27-cm) travel were used primarily, with 2-inch (5.08-cm) actuators used only to define the outer edge of the thicker boundary layers. The probes were alined by using a telescope mounted outside the plenum and a mirror in the plenum which allowed observation of the test section through the telescope. With this arrangement the magnified image of the pitot tube mouth could be alined with its reflection in the polished copper surface. This worked well with rectangular mouths but was not as useful with the round pitot mouths. Since the data were reproducible, as discussed later, the alinement procedure, was judged adequate.

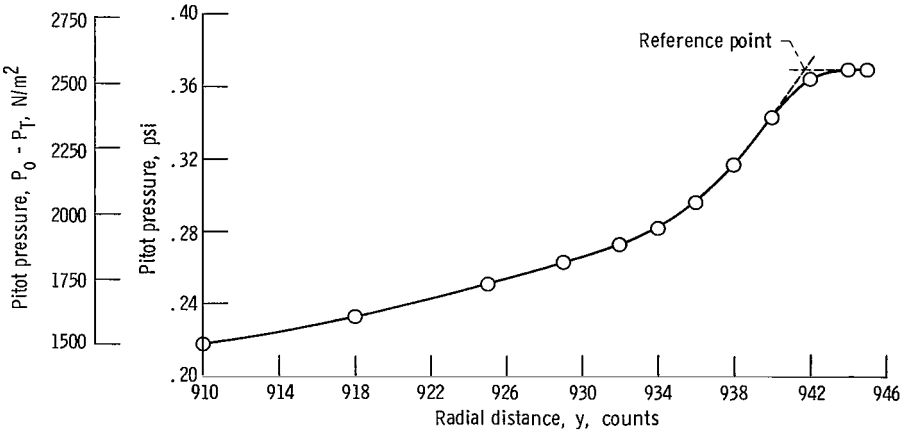

Figure 5. - Probe-wall contact determination for station 2. Free-stream Mach number, 0.24; 1 count = 0.0005 inch (0.00127 cm).

Contact between the probes and centerbody was indicated by an electrical short-circuit device. Early in the experiment it was discovered that, as a probe neared the centerbody, intermittent contact, due to probe vibration, was indicated. A typical pressure profile, measured near the wall, is shown in figure 5. As the centerbody was approached and contact was first indicated, the probe was at the inflection point in the profile. Further movement of the probe towards the centerbody caused the profile to flatten and the electrical short circuit to indicate full contact. The reference point, from which profile thickness parameters were measured, was taken as the intersection of the tangent, extrapolated from the inflection point, and the extended flat portion of the profile, as shown in figure 5. Accuracy of this technique, as judged from the figure, was approximately 0.0005 inch (0.00127 cm).

Differential strain gage pressure transducers, referenced to the plenum pressure, were used to read the pitot tube pressures. The range of the transducer used varied from 0.5 psid (3.450 kN/m^2) to 10 psid (68.950 kN/m^2), depending on the local differences between static and total pressures. A self-balancing potentiometer was used to read the thermocouple temperatures.

PROCEDURE AND DATA REDUCTION

Test Procedure

Prior to initiating the boundary-layer measurements, the static pressure distribution along the uncooled centerbody was determined without any probes in the test section. Comparison of this measurement with later tests, which included heat-transfer and

boundary-layer probes in the test section, indicated no observable effect due to wall cooling and no blockage effects due to reduction of flow passage area by the probe supports. The averaged result of a large number of measurements of the static to total-pressure ratio distribution is shown in figure 2. As a measure of the steady nature of this distribution, the maximum deviation from the average Mach number, corresponding to a measured static pressure, was 2.5 percent.

Using the control systems discussed in the APPARATUS section, approximately a half hour was required to attain steady-state conditions necessary for the measurements. A complete traverse of the boundary layer took approximately 1 hour, and was done in a step-wise fashion starting in the free-stream and moving towards the centerbody wall. Approximately 20 measurements were made during a traverse, with the step sizes decreasing progressively as the wall was approached. Care was taken at each step to insure that the probe pressure and temperature were steady and that the nominal plenum and wall temperatures had not changed significantly before continuing the traverse. Maximum allowable deviation from the nominal plenum and wall temperatures was 1° R (0.56 K) during a boundary-layer measurement with heat transfer. Larger deviations in plenum temperature were allowed during an adiabatic boundary-layer measurement, since the velocity profile is relatively insensitive to small temperature changes.

Heat-Transfer Measurement

Measurement of the heat transferred from the air to the nitrogen was attempted with a technique based on the known heat storage capacity of the copper wall, which has been used frequently elsewhere (refs. 9 and 10). Ideally, the measurement requires (1) quickly removing the coolant from the centerbody and (2) recording the rate of wall temperature increase. Because of the high thermal conductivity and thinness of the copper wall, a negligible temperature gradient exists in the radial direction. An energy balance on an element of wall (see appendix) yields the following relation for heat-transfer coefficient h.

$$h = \frac{b}{T_{aw} - T_w}\left[\rho C_p \frac{dT_w}{dt} - \frac{d}{dx}\left(k \frac{dT_w}{dx}\right)\right] \tag{1}$$

The wall thickness b, density ρ, specific heat C_p, and thermal conductivity k, were constant or known functions of the wall temperature T_w. Adiabatic wall temperature T_{aw} was easily measured, as was the steady-state wall temperature distribution in the axial x direction. The rate of temperature increase with time t at the instant the coolant was removed proved more difficult to measure, but the measurement was accom-

plished using an automatic voltage digitizer system which read each thermocouple at 0.75-second intervals.

When the experiment was designed, it was expected that the heat conduction term in equation (1) would be small relative to the heat-storage term, which is necessary for the measurement to be accurate. However, due primarily to blockage of the coolant flow passage by the instrument leads, the axial temperature distribution was not smooth. Also, the peak in this temperature distribution near the nozzle throat was sharper than expected. For these reasons, the magnitude of the second derivative in the conductive term could not be accurately evaluated, thus invalidating the heat-transfer measurement (see appendix).

Boundary-Layer Measurement

Mean velocity and temperature profiles were measured in the centerbody boundary layer using instruments described in the APPARATUS section. In the case of the adiabatic measurements, the boundary-layer total temperature was assumed to be constant, a normal and very accurate assumption (ref. 6) in the Mach number range considered here.

A small total-pressure recovery correction was applied to each pitot tube measurement. The correction factor was obtained by a measurement of the free-stream recovery pressure, P'_{Te} made during each test, and comparison with the plenum pressure. This method compared favorably with the independent calibration obtained for the probes. Since the correction

$$C \equiv \frac{P_T - P'_T}{P'_T - P} = \frac{P_o - P'_{Te}}{P'_{Te} - P} \tag{2}$$

is a weak function of Mach number, the value based on the free-stream measurement was used also within the boundary layer. In equation (2), P_T is the local total pressure, P'_T is the measured pressure, and P is the local static pressure. Maximum error due to this approximate correction procedure was estimated to be less than 1 percent in measured velocity. The boundary-layer thickness parameters were not affected significantly.

Recovery corrections were also made to the total temperature measurement using the correction factor, which is a function of Mach number,

$$\eta = \frac{T_R}{T_T} \tag{3}$$

where T_R is the measured temperature, and T_T is the local total temperature. Since the Mach number at each point in the boundary layer was determined by pressure measurement, no approximation for the correction procedure was necessary for the total temperature measurement. The correction factors obtained from the independent calibration, discussed in the APPARATUS section, were used in the data reduction process. These were checked during each test by comparison with an η based on the free-stream and plenum temperatures.

Knowing the centerbody static-pressure distribution, and the total pressure and temperature distributions at the five boundary-layer stations, the distributions of Mach number, static temperature, and sonic velocity could be determined from standard compressible flow relations (ref. 11). For Mach numbers greater than 0.3, the boundary-layer velocities were calculated from knowledge of the local sonic velocity and M. Below Mach 0.3, the incompressible form of Bernoulli's equation was used to calculate velocity, since in this range small errors in measured total pressure cause large errors in M and the corresponding velocity. At Mach 0.3, use of the Bernoulli equation results in an error of approximately 1 percent in velocity. The perfect gas law was used to calculate density wherever required.

Because the ratios of velocity and temperature thicknesses to the centerbody diameter were not always small, thin boundary-layer assumptions in the evaluation of the integral thickness parameters could not be accurately applied here. The alternative thick boundary-layer definitions for displacement thickness δ^*, momentum thickness θ, and energy thickness φ, used in this experiment were

$$\delta^*\left(1 + \frac{\delta^*}{2R}\right) = \int_0^{\delta,\,\Delta} \left(1 - \frac{\rho u}{\rho_e u_e}\right)\left(1 + \frac{y}{R}\right)dy \tag{4}$$

$$\theta\left(1 + \frac{\theta}{2R}\right) = \int_0^{\delta,\,\Delta} \frac{\rho u}{\rho_e u_e}\left(1 - \frac{u}{u_e}\right)\left(1 + \frac{y}{R}\right)dy \tag{5}$$

$$\varphi\left(1 + \frac{\varphi}{2R}\right) = \int_0^{\Delta} \frac{\rho u}{\rho_e u_e}\left(1 - \frac{T_T - T_w}{T_o - T_w}\right)\left(1 + \frac{y}{R}\right)dy \tag{6}$$

where ρ, u, and T_T are local density, velocity, and total temperature, respectively; ρ_e, u_e, and T_o are the corresponding free-stream values; T_w is the wall temperature; R is the centerbody radius; and y is the radial distance measured from the centerbody. The upper limit of integration in equations (4) and (5) was δ for the adiabatic wall

boundary layer and Δ for the cooled wall boundary layer. In every case the temperature boundary-layer thickness Δ was greater than the velocity thickness δ.

Use of the thin boundary-layer relations, instead of equations (4) to (6), resulted in values of δ^*, θ, and φ nearly 10 percent lower than those presented here for the upstream measuring stations. Of course, as the nozzle throat was approached, and the boundary layer became thinner, the differences between thick and thin boundary-layer calculations became insignificant.

It is important to note that a finite upper limit is used in equations (4) to (6), but in many places (ref. 12) an infinite upper limit (corresponding to free-stream conditions) would be used. In this experiment, it was preferred to use δ and Δ as upper limits, since significant differences in measured values of δ^*, θ, and φ occurred when different upper limits corresponding to free-stream conditions were used. These differences were attributable to the asymptotic character of the boundary-layer outer edge and the numerical integration technique used to evaluate the data. Use of infinite upper limits in equations (4) to (6), instead of those indicated, resulted in values for the integral thicknesses approximately 10 percent higher than those presented here.

No corrections for displacement effect were applied to the pitot tube measurements to be presented. As stated in reference 13, there is no question that errors due to displacement effect, and also turbulence, are real. However, it is not clear how the corrections are to be applied in every situation, since they have been derived from experiments using specialized probe goemetry and, in most cases, fully developed pipe flow. Disagreement on the magnitude of the corrections seemingly exists also. Reference 14 suggests a displacement correction equal to 0.19 times the outside thickness of the pitot tube; reference 15 suggests that no correction need be applied as long as the ratio of pitot thickness to velocity boundary-layer thickness is less than 0.29. Although, both round and rectangular pitot tubes, having different thicknesses, were used at the upstream stations in the present experiment, no outstanding differences between their measurements were noted. Since reference 14 suggests that differences should exist, particularly near the wall, the present experiment probably only further confuses the question of displacement effect corrections. As an example of the magnitude of error that may exist, the displacement correction of reference 14 was applied to an adiabatic measurement at the station nearest the nozzle throat, where the thinnest boundary layer was observed. The corrected value of displacement thickness was 18 percent higher than the uncorrected value, and the corresponding increase in momentum thickness was 10 percent. This is probably the maximum error due to displacement effect that could exist in this experiment since the ratio of pitot thickness to boundary-layer thickness is greatest at this station.

RESULTS AND DISCUSSION

Results of the boundary-layer measurements with and without heat transfer are presented in tables I and II. Only one set of data per station is given in each table, but at least two measurements were made at each test condition to confirm the experimental accuracy and obtain confidence in the instrumentation. Figures 6 and 7 present the same velocity and temperature profile data in graphical fashion. Temperature data are provided only for the cooled wall cases, since the total temperature was nearly constant throughout the adiabatic boundary layer. With the experimental results, predicted velocity and temperature profiles, calculated according to the method of reference 7, are shown. Average measured values of the various thickness parameters, from all the measurements at each station, are presented in figures 8 and 9 with the calculations from reference 7. Maximum deviation from the average was 9 percent for Δ at station 3 with heat transfer. Maximum deviation for an integral thickness was 7 percent for the adiabatic value of θ at station 5. Considering all stations, with and without heat transfer, the average maximum deviation for the various thickness parameters was about 3 percent. Also shown in figures 8 and 9 are values for friction coefficient C_f calculated by the cross-plot method suggested in reference 16 which makes use of the measured velocity profiles. These are also compared with the predictions using the technique of reference 7. Figure 9, in addition, shows the average measured axial temperature distribution with the curve fit approximation used in the computations.

The only noteworthy characteristic of the boundary-layer measurements not at least partly attributable to pressure gradient concerns the temperature profiles of figure 7. Comparison of the slopes of the experimental data to the predicted profiles near the wall shows that in every case the measured profiles are much steeper, indicating a possible direct heat-transfer effect between the probe thermocouple and the cooled wall. Since no method of evaluating the effect of heat transfer between the two bodies was known, no corrections for wall proximity were made to the reported temperature readings.

Pressure gradient effects were evaluated by comparing the experimental data to a prediction method (ref. 7) which uses a turbulent boundary-layer model based on flat-plate flow empiricism. The computational technique is a finite difference solution of the two dimensional, compressible boundary layer equations including pressure gradient. A mixing-length hypothesis is used to model the effective viscosity of turbulence in the region away from the wall. Near the wall, the eddy viscosity based on mixing length is combined in an exponential expression with the laminar viscosity so that the turbulent contribution is damped as the wall is approached. Two sets of initial conditions were applied to the computations shown in figures 8 and 9. In one case, integration of the boundary-layer equations was initiated at the first boundary-layer measuring station, $x = 2.50$ inches (6.35 cm), using the measured velocity and temperature profiles. The

TABLE I. - COOLED-WALL BOUNDARY-LAYER DATA

(a) Station 1; P_o = 29.38 in. Hg (99.01 kN/m^2); T_o = 642° R (357 K); u_e = 259.88 ft/sec (79.21 m/sec); T_w = 464° R (258 K); T_{aw} = 641° R (356 K); δ = 0.249 in. (0.632 cm); δ^*/δ = 0.0576; θ/δ = 0.0771; Δ/δ = 1.614; φ/δ = 0.129

Ratio of radial distance to boundary-layer velocity thickness, y/δ	Total to static pressure ratio, P_T/P	Boundary-layer temperature ratio, $\frac{(T_T - T_w)}{(T_o - T_w)}$	Boundary-layer velocity ratio, u/u_e	Ratio of radial distance to boundary-layer velocity thickness, y/δ	Total to static pressure ratio, P_T/P	Boundary-layer temperature ratio, $\frac{(T_T - T_w)}{(T_o - T_w)}$	Boundary-layer velocity ratio, u/u_e
0.015	1.0114	0.283	0.545	0.158	1.0233	0.779	0.842
.018	1.0126	.401	.585	.188	1.0244	.802	.865
.022	1.0135	.491	.615	.218	1.0252	.819	.881
.026	1 0147	.548	.646	.268	1.0267	.852	.911
.030	1.0156	.576	.668	.319	1.0275	.875	.928
0.034	1.0161	0.593	0.680	0.369	1.0283	0.892	0.943
.038	1.0165	.615	.692	.419	1.0289	.909	.955
.044	1.0171	.632	.706	.519	1.0295	.931	.967
.052	1.0177	.649	.721	.669	1.0301	.954	.980
.060	1.0184	.666	.736	.870	1.0304	.971	.988
0.070	1.0191	0.683	0.752	1.070	1.0306	0.977	0.991
.082	1.0198	.700	.768	1 271	1 0306	.982	.993
.098	1 0206	.723	.786	1.471	1.0307	.988	.995
118	1.0216	.740	805	1.848	1.0308	.994	.997
.138	1 0224	.756	.823	3 776	1.0309	.999	1.000

(b) Station 2; P_o 29 36 in. Hg (98.94 kN/m^2); T_o 638° R (354 K); u_e 290.22 ft/sec (88.46 m/sec); T_w 472° R (262 K); T_{aw} 637° R (354 K); δ 0 262 in. (0 665 cm); δ^*/δ 0.0500; θ/δ 0.0776; Δ/δ 1 893; φ/δ 0 158

Ratio of radial distance to boundary-layer velocity thickness, y δ	Total to static pressure ratio, P_T P	Boundary-layer temperature ratio, $\frac{(T_T - T_w)}{(T_o - T_w)}$	Boundary-layer velocity ratio, u u_e	Ratio of radial distance to boundary-layer velocity thickness, y δ	Total to static pressure ratio, PT P	Boundary-layer temperature ratio, $\frac{(T_T - T_w)}{(T_o - T_w)}$	Boundary-layer velocity ratio, u u_e
0.014	1.0153	0 286	0 567	0 240	1 0331	0 825	0 900
015	1 0160	.352	.585	288	1.0341	.849	916
.019	1 0180	.473	633	335	1 0349	867	930
023	1.0199	534	670	383	1.0356	.879	940
026	1.0209	.564	691	.478	1.0367	.910	958
0 032	1 0222	600	.716	.669	1.0377	.940	.975
040	1 0235	618	738	.859	1.0384	.958	986
049	1 0244	.649	755	1.050	1 0387	.970	.991
063	1 0254	667	772	1 241	1.0389	976	.994
078	1 0268	691	795	1 431	1.0389	.983	996
0 097	1.0280	715	816	1.799	1 0390	989	997
126	1.0293	746	838	3 623	1.0391	1 000	1 000
154	1.0304	776	857				
192	1 0321	800	883				

(c) Station 3; P_o 29 17 in. Hg (98.30 kN m^2); T_o 643° R (357 K); u_e 514.96 ft sec (156 96 m sec); T_w 484° R (269 K); T_{aw} 640° R (356 K); δ 0 187 in (0.475 cm); $\delta^* \delta$ 0 0119; $\theta \delta$ 0.0570; $\Delta \delta$ 1.813; $\varphi \delta$ 0 223

Ratio of radial distance to boundary-layer velocity thickness, y/δ	Total to static pressure ratio, P_T/P	Boundary-layer temperature ratio, $\frac{(T_T - T_w)}{(T_o - T_w)}$	Boundary-layer velocity ratio, u, u_e	Ratio of radial distance to boundary-layer velocity thickness, y/δ	Total to static pressure ratio, P_T/P	Boundary-layer temperature ratio, $\frac{(T_T - T_w)}{(T_o - T_w)}$	Boundary-layer velocity ratio, u/u_e
0.024	1 0830	0.332	0.740	0 197	1 1193	0.741	0.929
.025	1.0844	.383	.751	.250	1 1212	.767	.939
.031	1 0885	.478	779	.304	1.1227	799	.949
.036	1.0920	.536	.800	.370	1 1242	.824	957
.041	1.0951	.561	.815	.437	1.1253	.849	964
0.047	1 0981	0.574	0 829	0.531	1 1263	0.875	0.971
.052	1.1003	.587	.839	.705	1 1277	913	.981
.057	1.1023	600	.849	.972	1 1288	951	.990
.066	1.1045	.613	.859	1.239	1 1294	.970	.994
.076	1.1069	.626	.869	1.507	1.1296	.983	.996
0.087	1.1091	0.645	0.880	1.774	1.1297	.989	.997
.103	1.1115	.664	.891	2.042	1.1298	.996	.998
.130	1.1147	.684	.906	2 571	1.1298	1.002	.999
.156	1.1170	.716	.918	5.117	1.1298	1.008	1.000

TABLE I. - Concluded. COOLED-WALL BOUNDARY-LAYER DATA

(d) Station 4; P_o = 28.99 in. Hg (97.70 kN/m^2); T_o = 643^o R (357 K); u_e = 656.61 ft/sec (200.13 m/sec); T_w = 492^o R (273 K); T_{aw} = 638^o R (354 K); δ = 0.0797 in. (0.202 cm); δ^*/δ = 0.0222; θ/δ = 0.0548; Δ/δ = 3.149; φ/δ = 0.236

Ratio of radial distance to boundary-layer velocity thickness, y/δ	Total to static pressure ratio, P_T/P	Boundary-layer temperature ratio, $\frac{(T_T - T_w)}{(T_o - T_w)}$	Boundary-layer velocity ratio, u/u_e	Ratio of radial distance to boundary-layer velocity thickness, y/δ	Total to static pressure ratio, P_T/P	Boundary-layer temperature ratio, $\frac{(T_T - T_w)}{(T_o - T_w)}$	Boundary-layer velocity ratio, u/u_e
0.050	1.1454	0.438	0.769	0.376	1.2148	0.820	0.963
.056	1.1506	.539	.792	.439	1.2168	.840	.970
.069	1.1627	.587	.826	.596	1.2190	.881	.979
.082	1.1724	.615	.851	.753	1.2205	.908	.985
.094	1.1779	.636	.865	.910	1.2214	.928	.989
0.107	1.1821	0.649	0.876	1.223	1.2221	0.948	0.993
.125	1.1894	.677	.895	1.694	1.2228	.968	.996
.144	1.1942	.691	.906	2.321	1.2230	.981	.998
.169	1.1990	.711	.919	2.948	1.2230	.988	.999
.201	1.2030	.732	.929	3.262	1.2230	.991	1.000
0.232	1.2066	0.752	0.939	3.575	1.2230	0.995	1.000
.270	1.2096	.773	.947	3.889	1.2230	.995	1.000
.314	1.2121	.793	.955	4.203	1.2230	.995	1.000

(e) Station 5; P_o = 28.91 in. Hg (97.43 kN/m^2); T_o = 642^o R (357 K); u_e = 1105.50 ft/sec (336.96 m/sec); T_w = 509^o R (283 K); T_{aw} = 632^o R (351 K); δ = 0.0854 in. (0.217 cm); δ^*/δ = 0.0238; θ/δ = 0.0575; Δ/δ = 2.658; φ/δ = 0.298

Ratio of radial distance to boundary-layer velocity thickness, y/δ	Total to static pressure ratio, P_T/P	Boundary-layer temperature ratio, $\frac{(T_T - T_w)}{(T_o - T_w)}$	Boundary-layer velocity ratio, u/u_e	Ratio of radial distance to boundary-layer velocity thickness, y/δ	Total to static pressure ratio, P_T/P	Boundary-layer temperature ratio, $\frac{(T_T - T_w)}{(T_o - T_w)}$	Boundary-layer velocity ratio, u/u_e
0.043	1.4074	0.315	0.710	0.430	1.8136	0.807	0.973
.049	1.4397	.439	.743	.518	1.8181	.838	.978
.061	1.4863	.495	.778	.664	1.8226	.868	.984
.073	1.5199	.512	.800	.811	1.8241	.899	.987
.084	1.5497	.529	.818	.957	1.8252	.914	.989
0.096	1.5781	0.545	0.836	1.162	1.8265	0.937	0.992
.114	1.6105	.562	.855	1.496	1.8274	.960	.995
.131	1.6415	.579	.872	2.128	1.8277	.983	.998
.155	1.6713	.603	.889	2.714	1.8278	.991	.998
.178	1.6991	.627	.905	3.300	1.8278	.998	.999
0.207	1.7269	0.658	0.920	3.885	1.8278	1.006	1.000
.237	1.7496	.682	.933	4.471	1.8278	1.006	1.000
.272	1.7735	.714	.947	5.056	1.8278	1.006	1.000
.313	1.7916	.752	.958	5.624	1.8278	1.006	1.000
.371	1.8065	.784	.968				

TABLE II. - ADIABATIC BOUNDARY-LAYER DATA

(a) Station 1; P_o = 29.45 in. Hg (99.25 kN/m^2); T_o = 641^o R (356 K); u_e = 259.69 ft/sec (79.15 m/sec); δ = 0.224 in. (0.569 cm); δ^*/δ = 0.0946; θ/δ = 0.0714

Ratio of radial distance to boundary-layer velocity thickness, y/δ	Total to static pressure ratio, P_T/P	Boundary-layer velocity ratio, u/u_e	Ratio of radial distance to boundary-layer velocity thickness, y/δ	Total to static pressure ratio, P_T/P	Boundary-layer velocity ratio, u/u_e
0.017	1.0095	0.555	0.184	1.0219	0.842
.019	1.0103	.578	.218	1.0229	.862
.024	1.0117	.618	.251	1.0240	.882
.028	1.0128	.646	.295	1.0253	.906
.033	1.0137	.666	.351	1.0266	.928
0.037	1.0142	0.680	0.429	1.0278	0.948
.044	1.0150	.697	.574	1.0291	.970
.050	1.0156	.713	.797	1.0300	.985
.059	1.0162	.726	1.020	1.0303	.991
.073	1.0170	.744	1.243	1.0306	.994
0.088	1.0178	.761	1.465	1.0306	0.995
.106	1.0186	.776	1.688	1.0307	.996
.128	1.0198	.800	2.049	1.0308	.998
.155	1.0209	.822	3.471	1.0309	1.000

(b) Station 2; P_o = 29.44 in. Hg (99.21 kN/m^2); T_o = 632^o R (351 K); u_e = 289.46 ft/sec (88.23 m/sec); δ = 0.223 in. (0.566 cm); δ^*/δ = 0.0919; θ/δ = 0.0713

Ratio of radial distance to boundary-layer velocity thickness, y/δ	Total to static pressure ratio, P_T/P	Boundary-layer velocity ratio, u/u_e	Ratio of radial distance to boundary-layer velocity thickness, y/δ	Total to static pressure ratio, P_T/P	Boundary-layer velocity ratio, u/u_e
0.017	1.0130	0.579	0.268	1.0316	0.900
.022	1.0150	.621	.325	1.0328	.917
.026	1.0169	.661	.381	1.0337	.930
.031	1.0185	.691	.437	1.0347	.943
.035	1.0196	.710	.504	1.0354	.952
0.040	1.0203	0.722	0.616	1.0366	0.968
.046	1.0210	.735	.785	1.0375	.981
.055	1.0219	.751	1.009	1.0383	.990
.071	1.0233	.774	1.233	1.0388	.996
.089	1.0244	.792	1.458	1.0389	.998
0.111	1.0259	0.816	1.682	1.0391	1.000
.134	1.0269	.831	1.907	1.0391	1.000
.167	1.0283	.852	2.046	1.0391	1.000
.212	1.0299	.876			

(c) Station 3; P_o 29.28 in. Hg (98.67 kN/m^2); T_o 659^o R (366 K); u_e 520.84 ft/sec (158.75 m/sec); δ 0.113 in. (0.287 cm); δ^*/δ 0.0635; θ/δ 0.0403

Ratio of radial distance to boundary-layer velocity thickness, y/δ	Total to static pressure ratio, P_T/P	Boundary-layer velocity ratio, u/u_e	Ratio of radial distance to boundary-layer velocity thickness, y/δ	Total to static pressure ratio, P_T/P	Boundary-layer velocity ratio, u/u_e
0.047	1.0862	0.825	0.238	1.1150	0.945
.051	1.0878	.833	.273	1.1163	.950
.060	1.0907	.845	.326	1.1185	.959
.069	1.0940	.860	.393	1.1202	.965
.078	1.0969	.872	.481	1.1217	.971
0.087	1.0989	0.881	0.592	1.1235	0.977
.096	1.1012	.890	.747	1.1253	.984
.109	1.1039	.901	1.035	1.1273	.991
.122	1.1060	.910	1.478	1.1289	.997
.136	1.1077	.917	1.921	1.1296	999
0.153	1.1094	0.923	2.364	1.1298	1.000
.171	1.1108	.929	2.808	1.1298	1.000
.189	1.1122	.935	3.251	1.1298	1.000
.211	1.1137	.940	3.694	1.1298	1.000

TABLE II. - Concluded. ADIABATIC BOUNDARY-LAYER DATA

(d) Station 4; P_o = 29.43 in. Hg (99.18 kN/m^2); T_o = 655° R (364 K); u_e = 663.98 ft/sec (202.38 m/sec); δ = 0.0468 in. (0.119 cm); δ^*/δ = 0.0921; θ/δ = 0.0425

Ratio of radial distance to boundary-layer velocity thickness, y/δ	Total to static pressure ratio, P_T/P	Boundary-layer velocity ratio, u/u_e	Ratio of radial distance to boundary-layer velocity thickness, y/δ	Total to static pressure ratio, P_T/P	Boundary-layer velocity ratio, u/u_e
0.113	1.1555	0.850	0.482	1.2091	0.971
.119	1.1583	.857	.557	1.2120	.977
.140	1.1658	.875	.664	1.2149	.983
.161	1.1729	.892	.878	1.2178	.988
.183	1.1792	.906	1.145	1.2196	.992
0.204	1.1827	0.914	1.680	1.2219	0.996
.226	1.1871	.924	2.214	1.2229	.998
.247	1.1898	.930	2.749	1.2233	.999
.279	1.1939	.939	3.284	1.2236	1.000
.311	1.1965	.944	3.818	1.2237	1.000
0.343	1.1988	0.949	4.353	1.2237	1.000
.386	1.2027	.957	4.887	1.2237	1.000
.429	1.2056	.963	5.422	1.2237	1.000
			5.957	1.2237	1.000

(e) Station 5; P_o = 29.26 in. Hg (98.61 kN/m^2); T_o = 646° R (359 K); u_e = 1108.06 ft/sec (337.74 m/sec); δ = 0.0336 in. (0.0853 cm); δ^*/δ = 0.137; θ/δ = 0.0604

Ratio of radial distance to boundary-layer velocity thickness, y/δ	Total to static pressure ratio, P_T/P	Boundary-layer velocity ratio, u/u_e	Ratio of radial distance to boundary-layer velocity thickness, y/δ	Total to static pressure ratio, P_T/P	Boundary-layer velocity ratio, u/u_e
0.113	1.3921	0.755	1.065	1.8079	0.992
.128	1.4179	.775	1.363	1.8143	.994
.158	1.4719	.813	1.735	1.8182	.996
.187	1.5080	.837	2.107	1.8207	.997
.232	1.5492	.862	2.627	1.8227	.998
0.277	1.5865	0.884	3.594	1.8246	0.999
.321	1.6225	.903	5.082	1.8260	.999
.366	1.6599	.923	6.570	1.8267	1.000
.426	1.6972	.941	8.058	1.8270	1.000
.500	1.7319	.958	9.545	1.8274	1.000
0.574	1.7500	0.966	11.033	1.8274	1.000
.693	1.7718	.976	12.521	1.8274	1.000
.842	1.7937	.986	13.369	1.8274	1.000

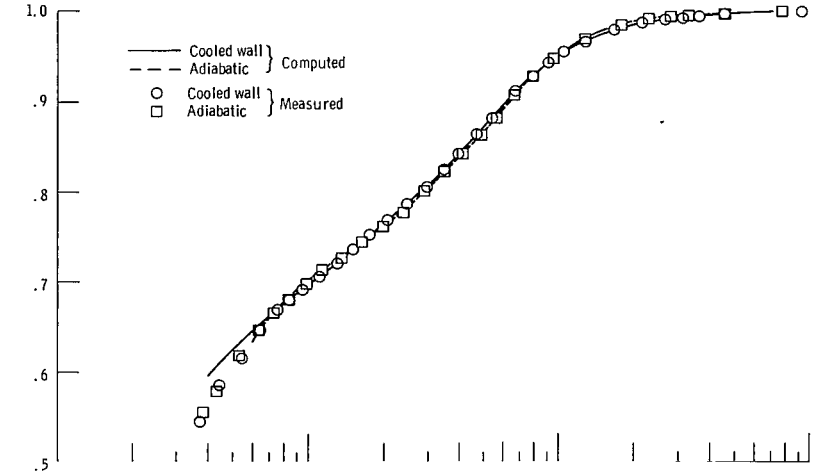

(a) Station 1; free-stream Mach number, 0.21.

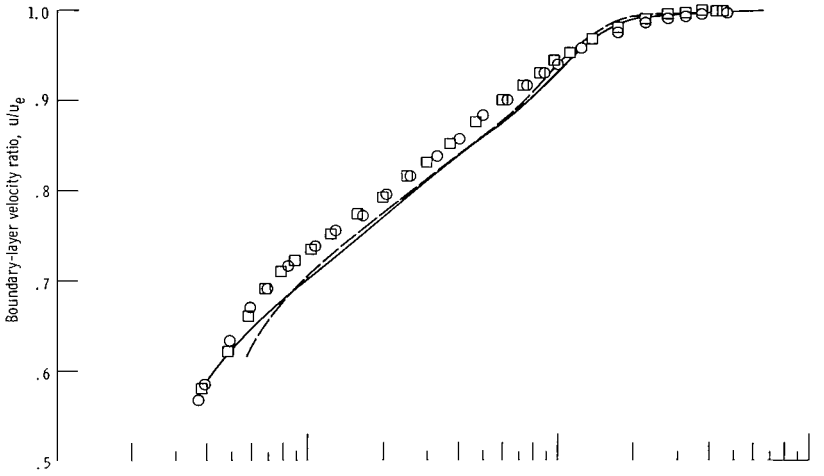

(b) Station 2; Free-stream Mach number, 0.24.

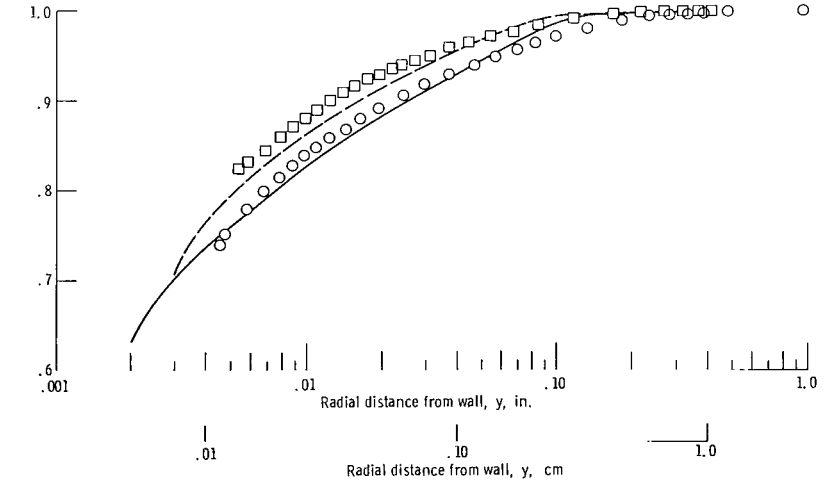

(c) Station 3; free-stream Mach number, 0.42.

Figure 6. - Boundary-layer velocity distributions.

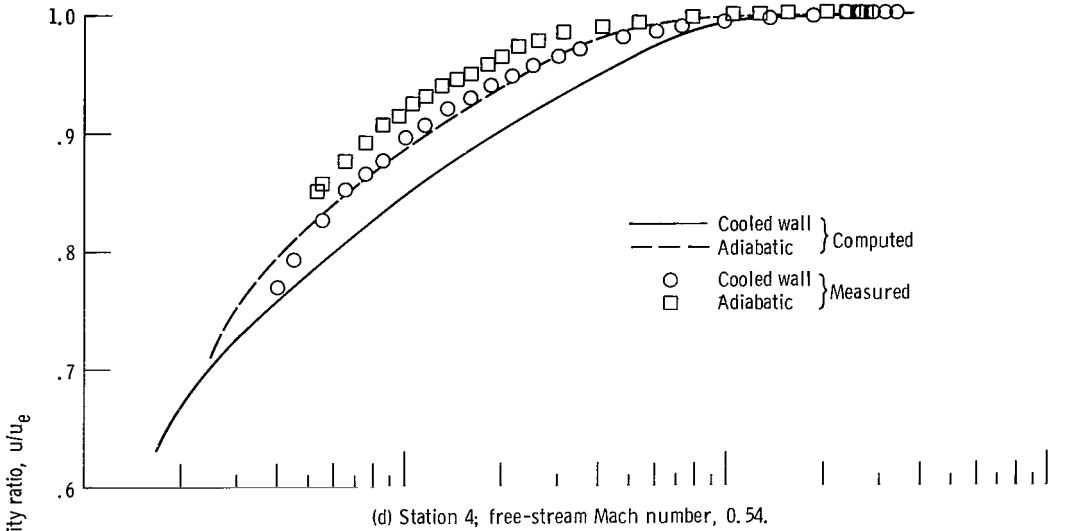

(d) Station 4; free-stream Mach number, 0.54.

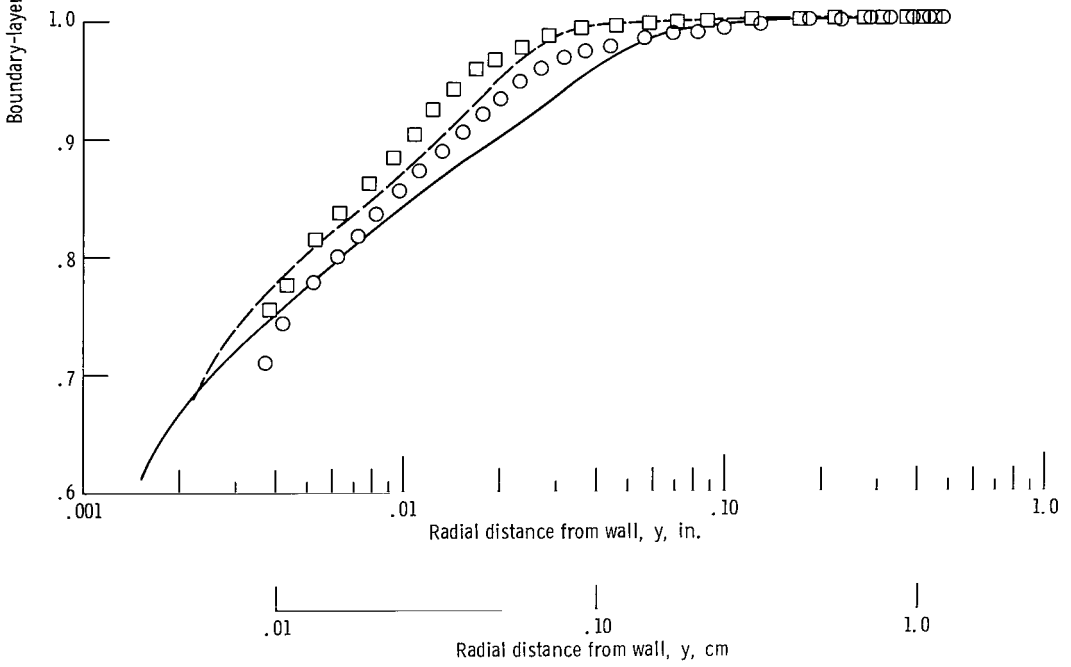

(e) Station 5; free-stream Mach number, 0.97.

Figure 6. - Concluded.

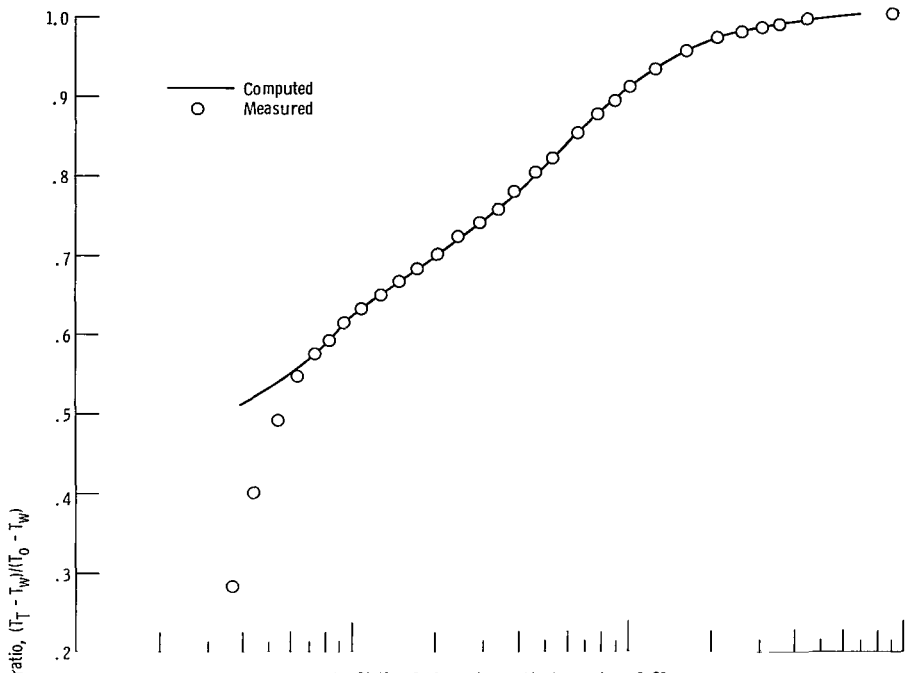

(a) Station 1; free-stream Mach number, 0.21.

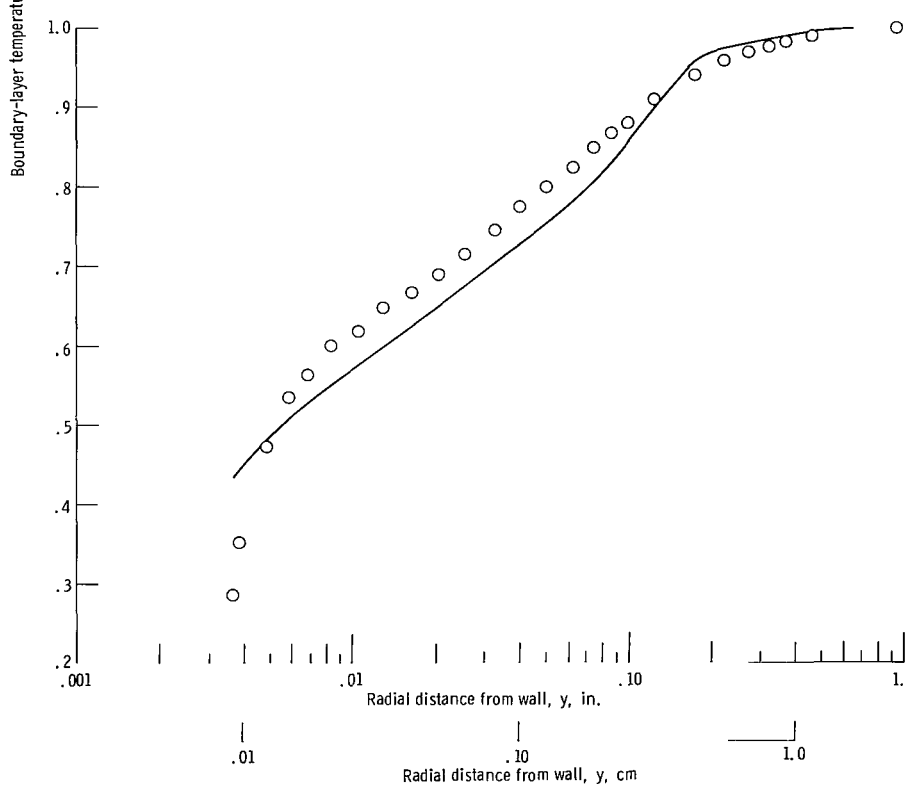

(b) Station 2; free-stream Mach number, 0.24.

Figure 7. - Boundary-layer temperature distributions.

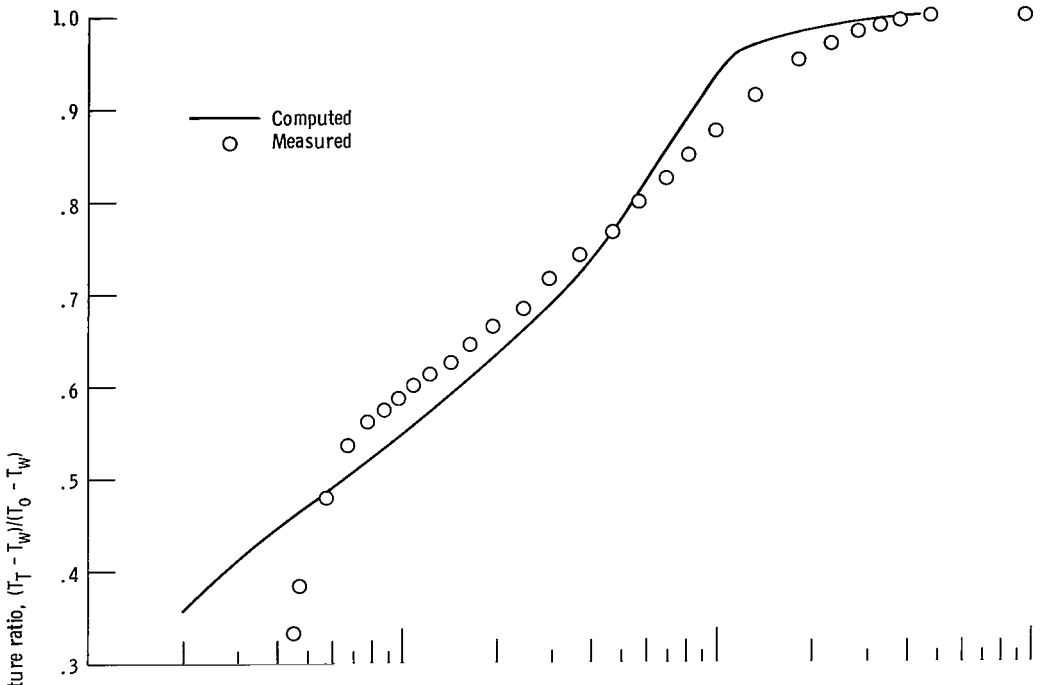

(c) Station 3; free-stream Mach number, 0.42.

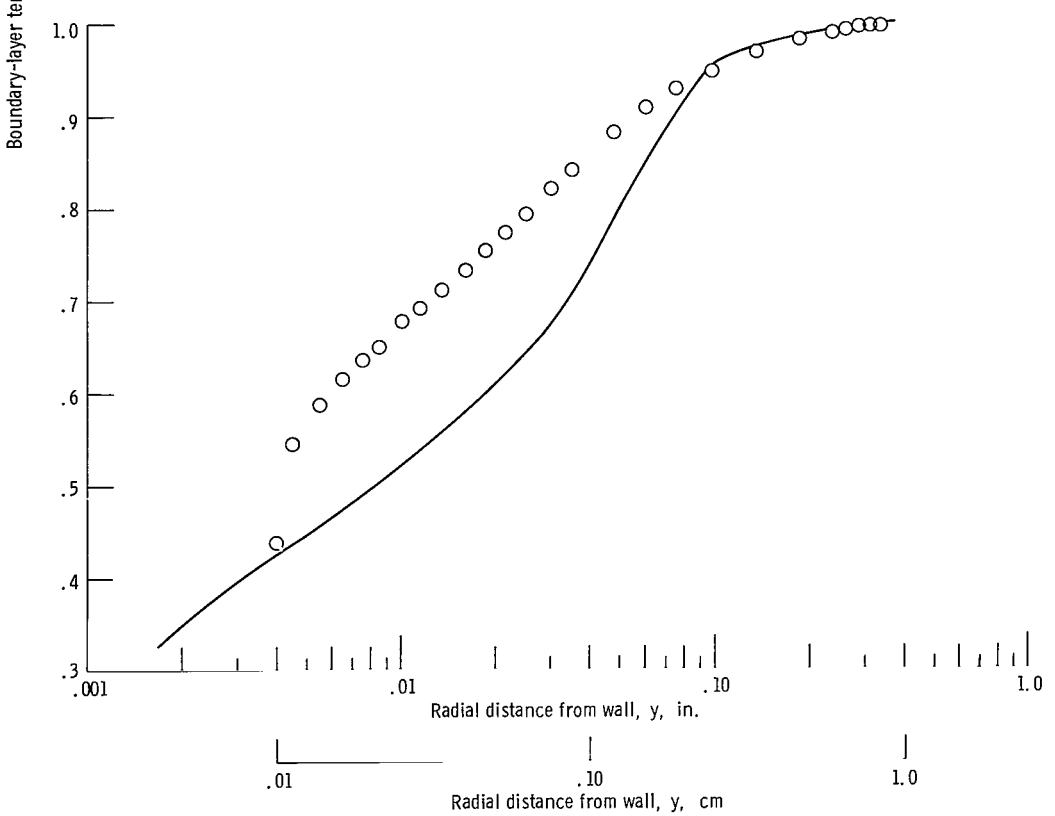

(d) Station 4; free stream Mach number, 0.54.

Figure 7. - Continued.

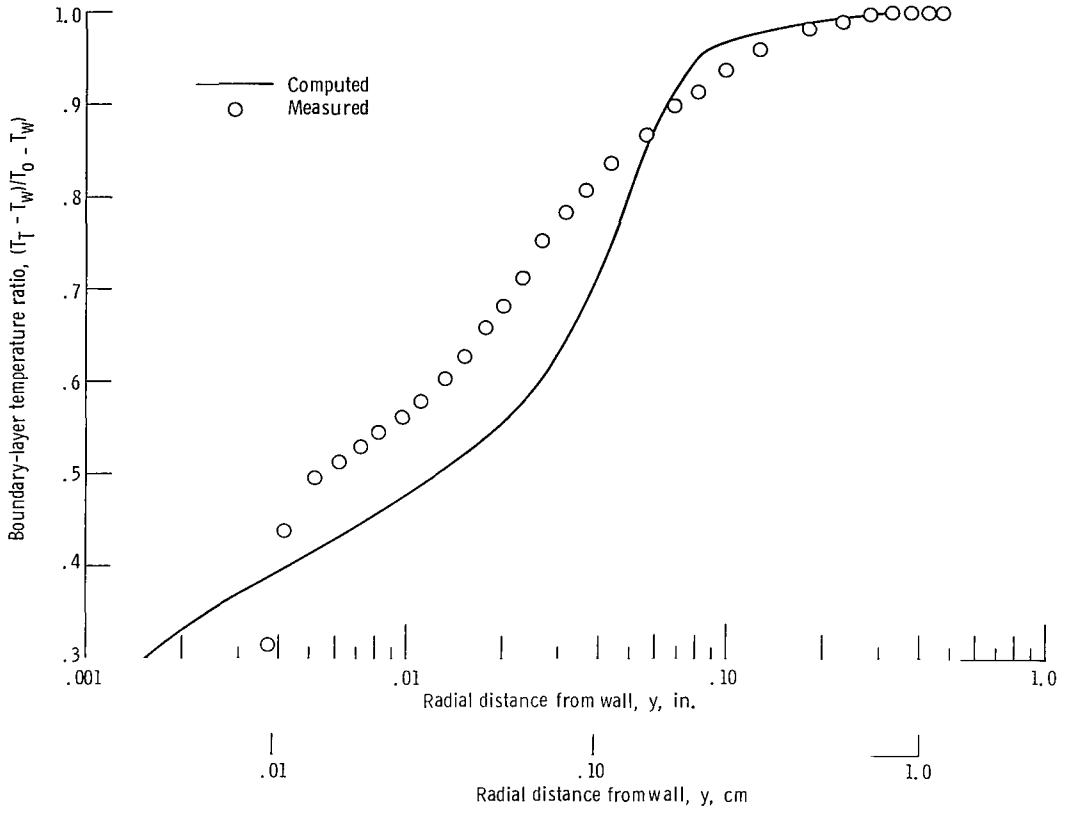

(e) Station 5; free-stream Mach number, 0.97.

Figure 7. - Concluded.

other initialization used velocity and temperature profiles extrapolated from the experimental data at $x = 2.50$ inches (6.35 cm) to $x = 0$. Only the results from the first initialization scheme are indicated in figures 6 and 7.

Pressure gradient effects have recently been discussed in terms of an acceleration parameter suggested in reference 3 and defined as follows:

$$K = \frac{\nu_e}{u_e^2} \frac{du_e}{dx} \tag{7}$$

This parameter is very convenient because it is defined in terms of conditions external to the boundary layer, and, therefore, is easily measured. As stated in reference 4, values for K between 2×10^{-6} and 3.5×10^{-6} have been suggested as criteria for the occurrence of laminarization. Figure 2 shows the range of K observed in this experiment with the measured pressure distribution and the curve fit approximation used in the integration of the boundary layer equations. Since the highest value of the acceleration

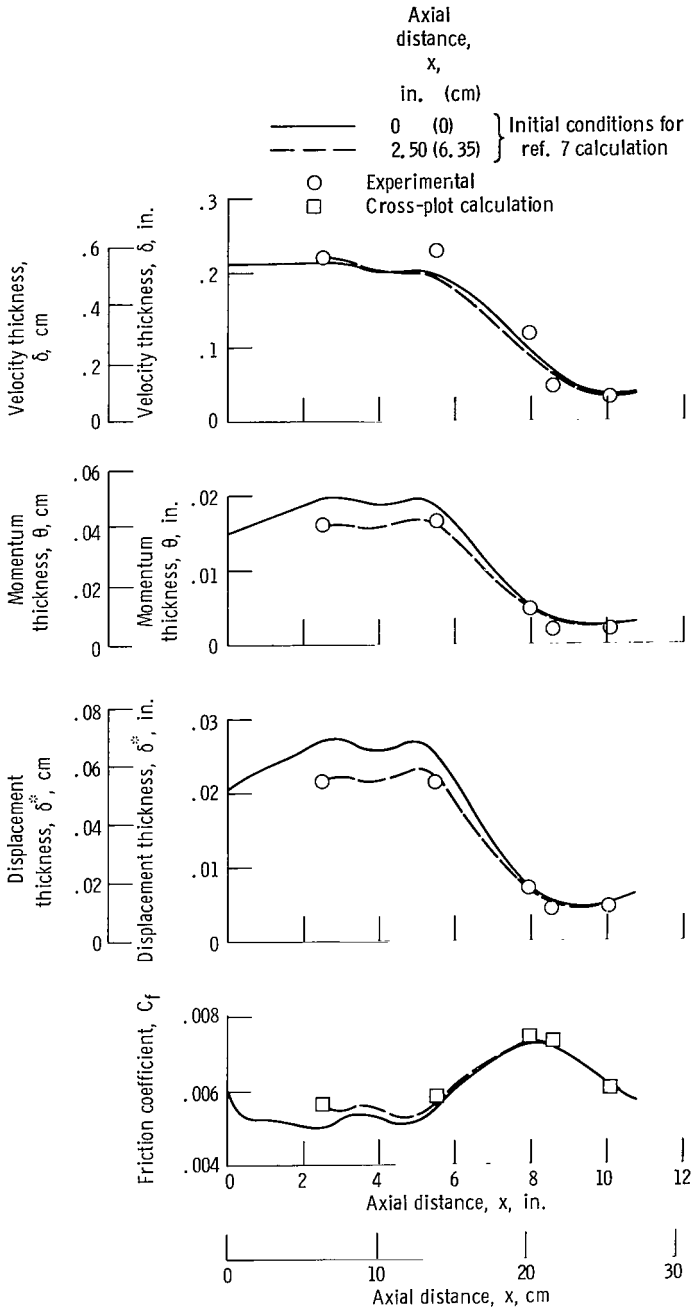

Figure 8. - Adiabatic experimental data and calculation results.

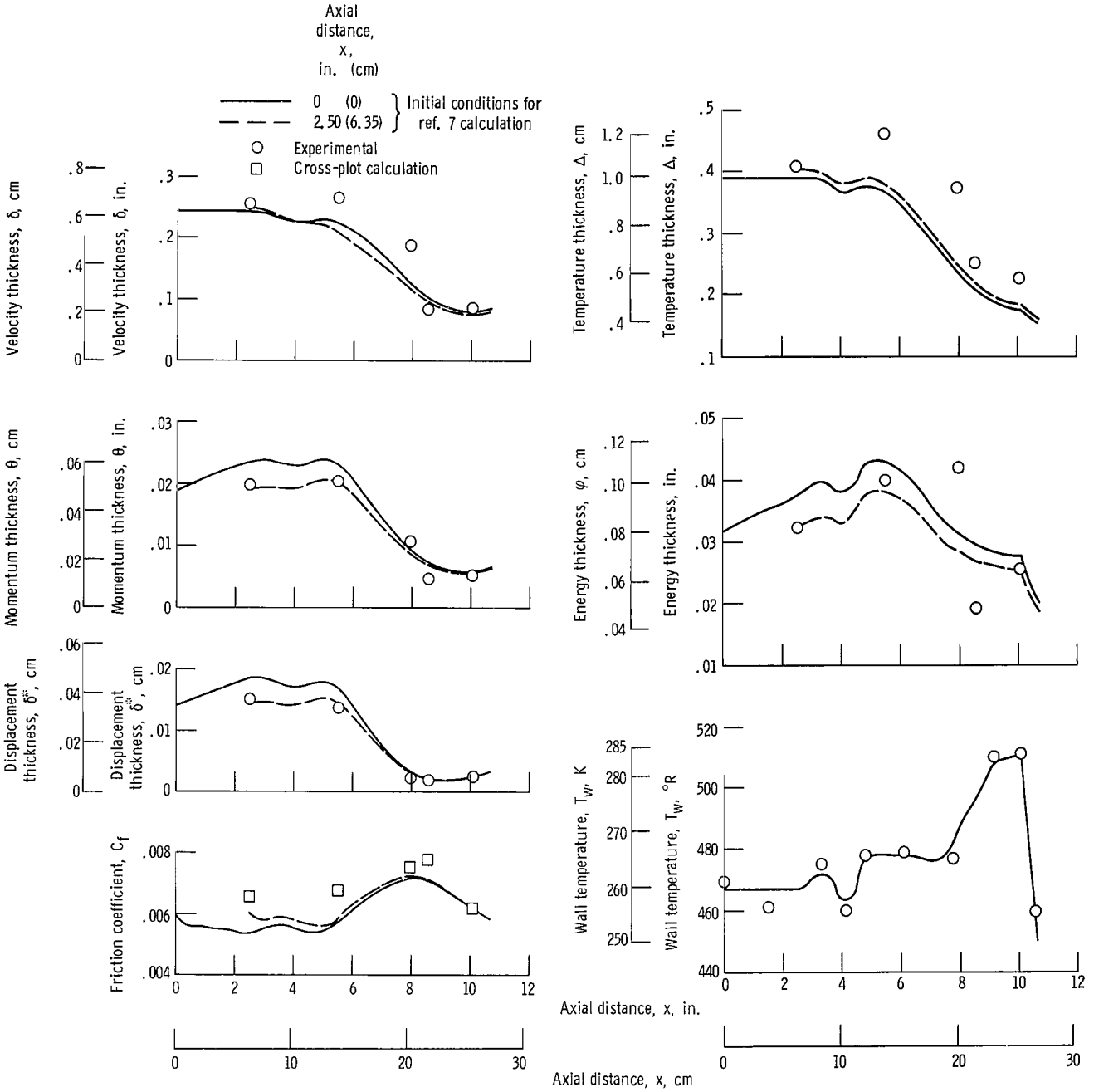

Figure 9. - Cooled-wall experimental data and calculation results.

parameter was about 2.3×10^{-6}, it cannot be stated definitely that laminarization did occur. However, as indicated in references 2, 4, and 6, significant reductions in heat transfer below the level normally associated with a turbulent boundary layer are to be expected with the values of K observed in the present experiment.

As indicated in figure 6, the strong favorable pressure gradient causes the wake component of the velocity profiles (ref. 12) to disappear as K increases from about 0.1×10^{-6} at station 1 to 2.2×10^{-6} at station 3. At station 5, K has decreased to about 0.9×10^{-6}, and a slight wake component can be observed again in the velocity profiles. These trends are evident in the predicted as well as the measured profiles, with and without heat transfer. The temperature profiles shown in figure 7 do not indicate the same trends as the corresponding velocity profiles. A wake component exists in all of the measured temperature profiles, although at station 4 it is very slight. The predicted profiles indicate a wake which progressively becomes a greater portion of the profile as the flow progresses from the inlet to the nozzle throat.

As stated in reference 4, the decrease in heat transfer observed for accelerated flows is believed to result from a combination of the effects of a thicker sublayer and a thermal boundary layer penetrating beyond the momentum boundary layer. This is demonstrated in reference 4 through arguments involving the integral forms of the boundary-layer momentum and energy equations. It is shown that for sufficiently large values of K a decrease in Reynolds number based on momentum thickness occurs. However, under the same conditions the energy thickness Reynolds number continues to increase, which means that the thermal boundary layer grows outside the momentum layer into a region of low eddy conductivity and high resistance to heat transfer. This result is also demonstrated in reference 2.

In the present experiment the effect of acceleration was to reduce the thickness of the momentum boundary layer, and the effect of cooling was to increase the velocity and momentum thicknesses and decrease the displacement thickness. At station 5 the velocity thickness for the cooled boundary layer was about 2.7 times thicker than the corresponding adiabatic measurement, and the cooled boundary layer momentum thickness was about 2.5 times the adiabatic thickness. This increase only shows the interdependence of the boundary-layer energy and momentum equations, since the thicker momentum layer in the heat-transfer case was due to the thick thermal layer which was not as severely affected by the acceleration, thereby agreeing with the argument of reference 4.

The observed nature of the wake components of the boundary layer and the actual thickness measurements indicate that the thermal boundary layer does indeed become much thicker than the momentum layer as the flow is accelerated. The ratio φ/θ increased from 1.6 at station 1 to 5.1 at station 5. The fact that φ was considerably larger than θ even at station 1 was probably due to the acceleration caused by the bellmouth inlet. These results compare favorably with the measurements of refer-

ences 2 and 4. Considering the case where the calculation of reference 7 was initialized at the first boundary-layer measuring station, the predicted value of φ/θ at station 5 was 4.5. Thus, even the flat-plate flow empiricism used here to model the effective viscosity qualitatively predicted the rapid growth of the thermal boundary layer relative to the momentum layer due to acceleration. However, as indicated above, the shapes of the measured temperature profiles differ somewhat from the predictions of reference 7 in the region of highest acceleration, resulting in a 12-percent difference between the measured and predicted values of φ/θ near the nozzle throat. Therefore, the mixing length hypothesis, particularly as it pertains to the accelerating thermal boundary layer, probably has not been an effective model and should be reexamined.

The argument of reference 4 pertaining to the sublayer growth with acceleration can be examined by investigating the measurements and predictions in universal or "law of the wall" coordinates in figures 10 and 11 where

$$y^+ = \frac{yu_t}{\nu_w} \tag{8}$$

$$u^+ = \frac{u}{u_t} \tag{9}$$

$$T^+ = \frac{C_f u_e}{2Stu_\tau}\left(\frac{T_T - T_w}{T_{aw} - T_w}\right) \tag{10}$$

where u_τ is the commonly used shear velocity based on wall conditions (ref. 12). Values of friction coefficient C_f and Stanton number St from reference 7 were used with the experimental data in figures 10 and 11. Also shown in these figures is a representation of the law of the wall (ref. 12) in order to better compare the present results with those from flat-plate flow analysis. The form used here is due to Clauser (ref. 16) and can be written

$$u^+ = T^+ = 2.44 \ln y^+ + 4.9 \tag{11}$$

The assumption that $u^+ = T^+$ in equation (11) implies unit Prandtl number, which is not important in the discussion to follow.

In terms of the universal coordinates, it is often assumed that the laminar or molecular viscosity can be ignored beyond $y^+ = 26$ (refs. 4 and 7). This value is based on flat-plate flow empiricism. Below $y^+ = 26$, it is assumed that a buffer layer, where turbulent and laminar viscosities are important, exists, and, very near the wall, a

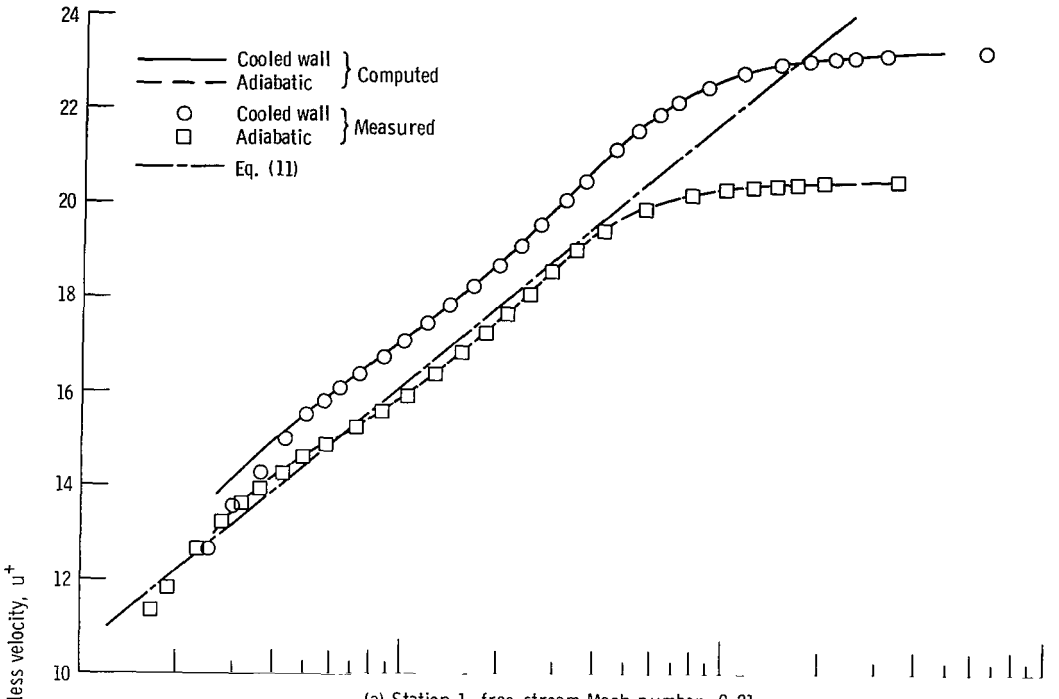

(a) Station 1; free-stream Mach number, 0.21.

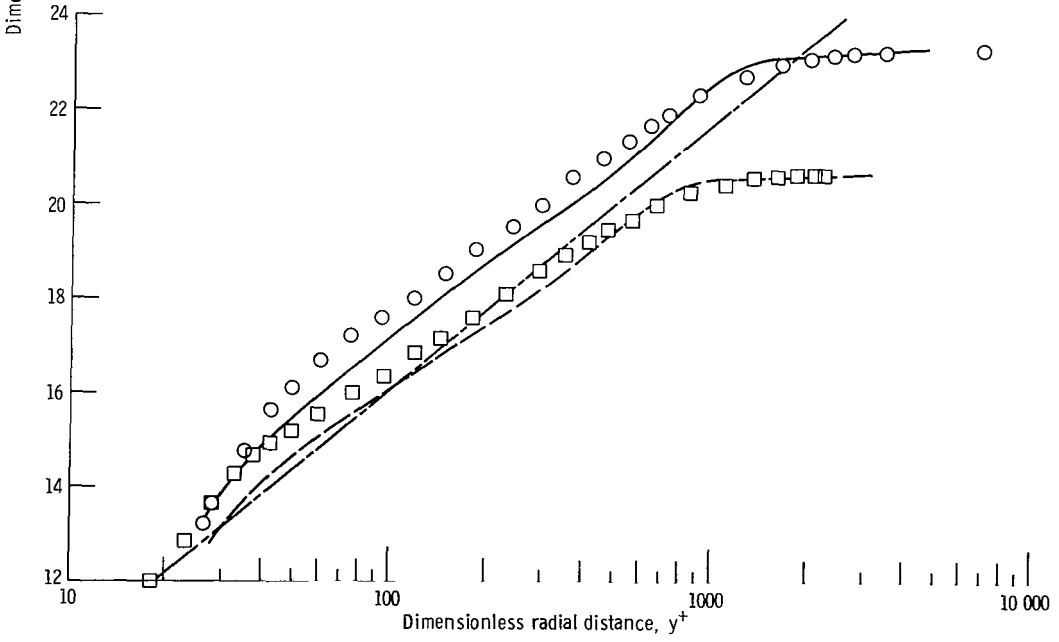

(b) Station 2; free-stream Mach number, 0.24.

Figure 10. - Dimensionless velocity profiles.

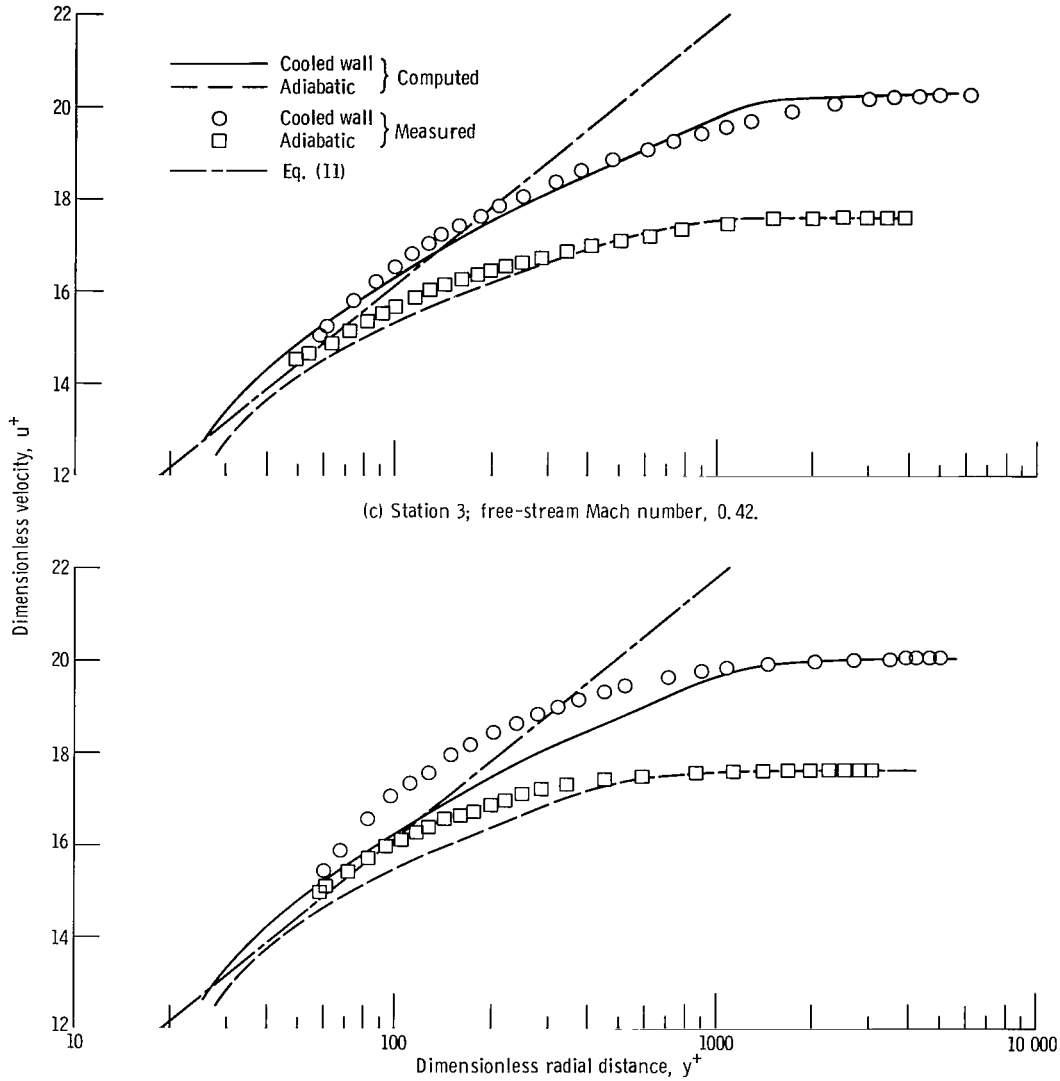

(c) Station 3; free-stream Mach number, 0.42.

(d) Station 4; free-stream Mach number, 0.54.

Figure 10. - Continued.

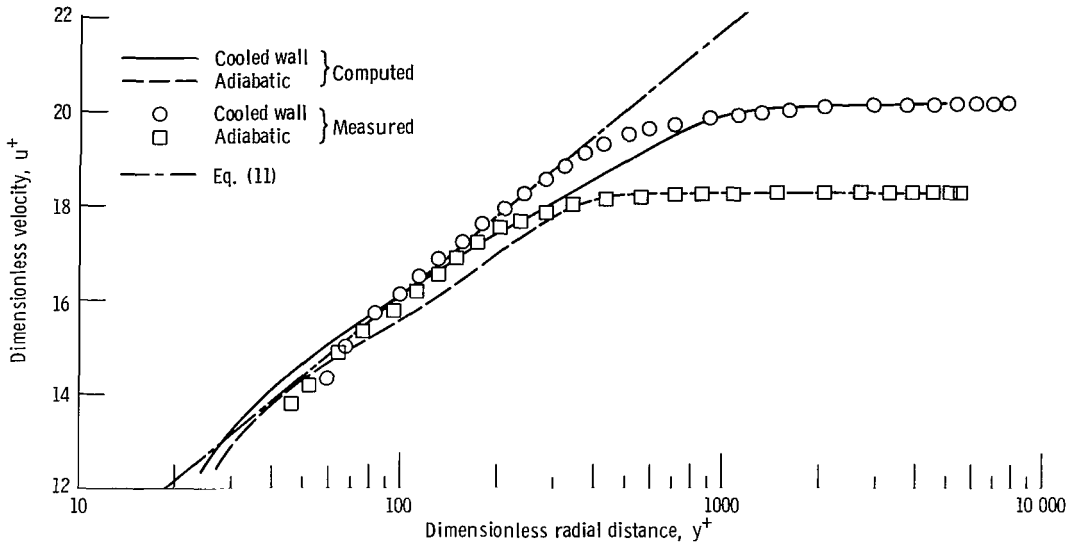

(e) Station 5; free-stream Mach number, 0.97.

Figure 10. - Concluded.

completely laminar sublayer is assumed. As stated previously, reference 7 combines these two regions into one sublayer model, which is the method suggested also in reference 4. The existence of this sublayer is characterized by a sudden increase in the slope of a velocity or temperature profile from that predicted by the law of the wall (eq. (11)) as the wall is approached.

Because of the thinness of the measured momentum boundary layer, particularly in the region of high acceleration, it is difficult to state for certain what the extent of the velocity sublayer was in the present experiment. At stations 3 and 4, the measured velocity profiles indicate no definite law of the wall region, and what was measured might be termed a wake-like flow for highly accelerated boundary layers. The other three stations, as discussed previously, have more standard type velocity profiles, including the same type of wake region as observed in zero or adverse pressure gradient flows. However, these three stations also indicate the possible extent of the sublayer. At the two upstream stations, where the acceleration is slight, the measured sublayer seemingly extends to about $y^+ = 40$, whereas, at the far downstream station, the sublayer might extend to as far as $y^+ = 70$. This is essentially the same with or without heat transfer. The values of y^+ stated here, however, must be considered highly qualitative, since wall friction was not measured.

The measured thermal boundary layer could provide more definite information as to the extent of the temperature sublayer if the possibility of significant heat transfer between the probe and centerbody wall did not exist. From figure 11, it appears that the sublayer extends to about $y^+ = 40$ at the two upstream stations and to about $y^+ = 80$ for

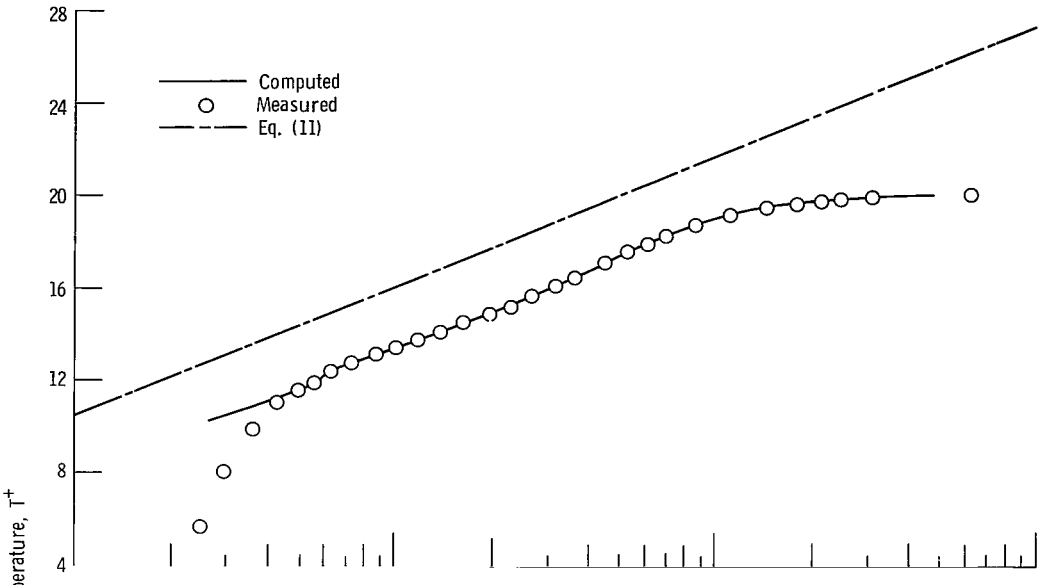

(a) Station 1; free-stream Mach number, 0.21.

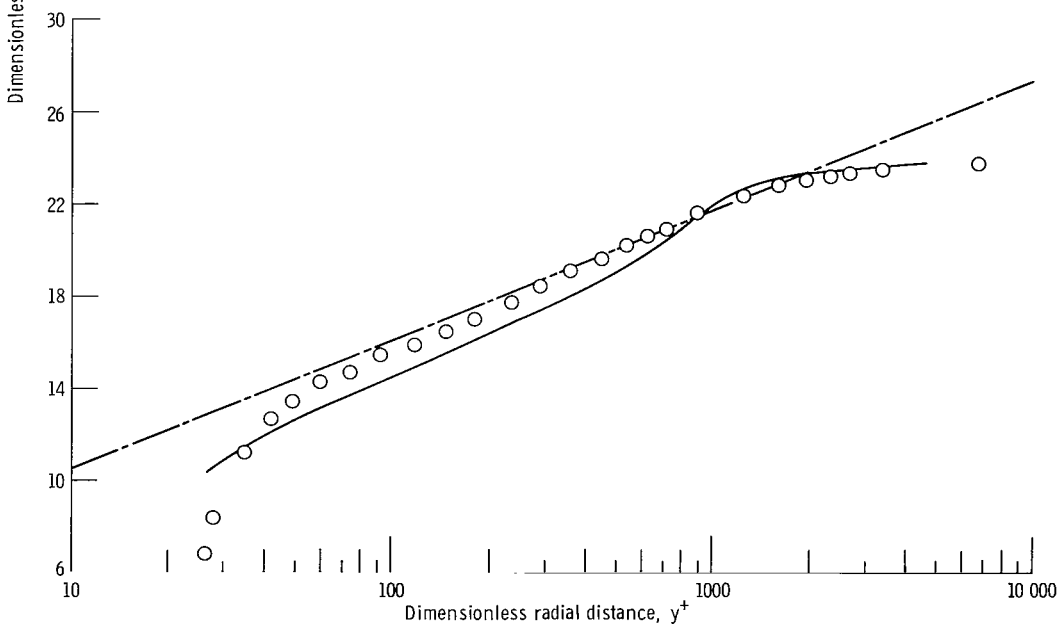

(b) Station 2; free-stream Mach number, 0.24.

Figure 11. - Dimensionless temperature profiles.

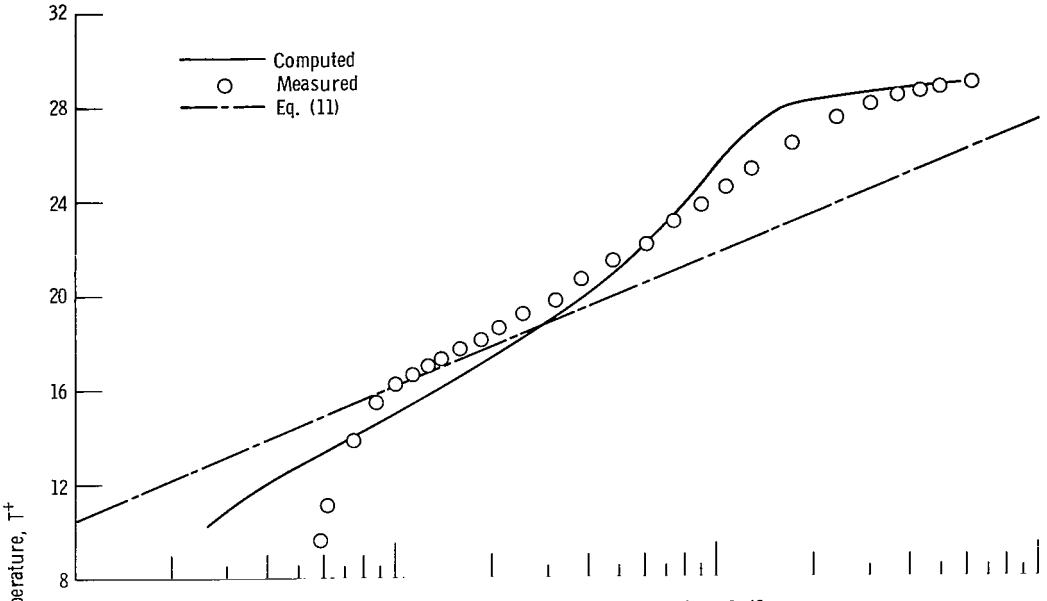

(c) Station 3; free-stream Mach number, 0.42.

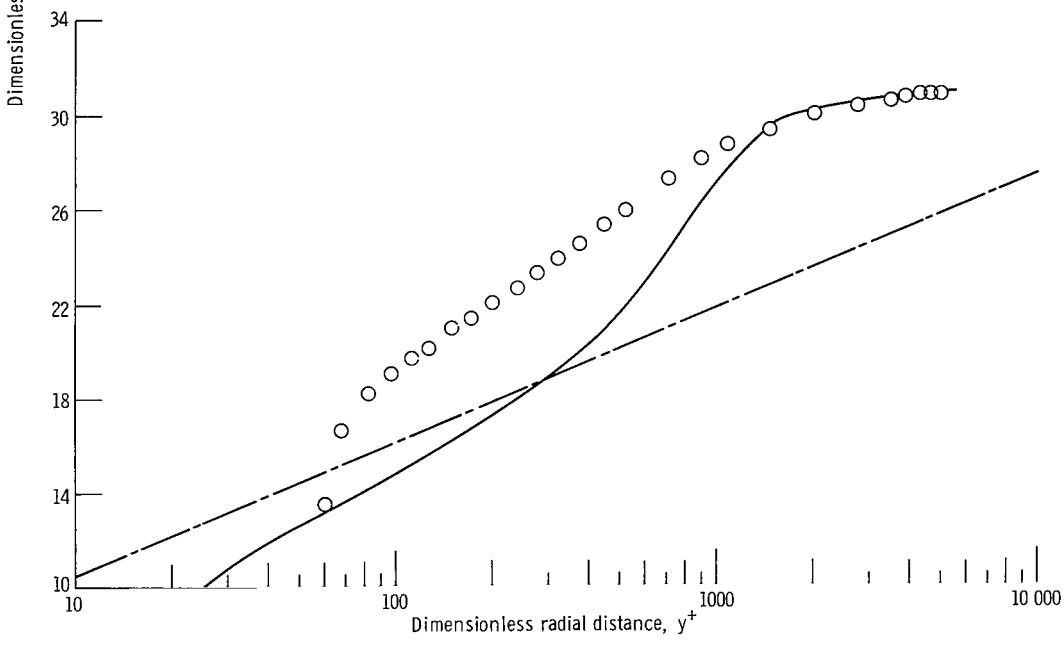

(d) Station 4; free-stream Mach number, 0.54.

Figure 11. - Continued.

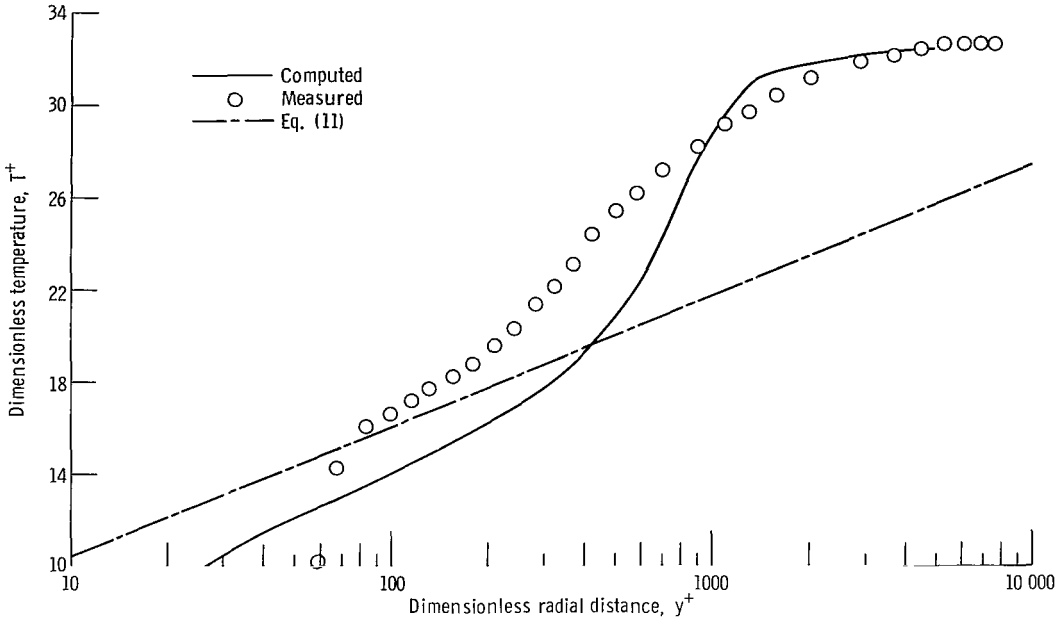

(e) Station 5; free-stream Mach number, 0.97.

Figure 11. - Concluded.

the three downstream stations. This is very similar to the extent of the sublayers noted above for the three velocity profiles where a noticeable sublayer existed. If this were true, then it could be asserted that a definite increase in the extent of the sublayer was caused by the acceleration. However, the possible heat-transfer effect between probe and wall, and, also, the fact that the actual wall friction is not known, somewhat cloud the issue.

The predicted velocity and temperature profiles of reference 7 (as indicated in figs. 10 and 11) give no indication of any sublayer growth as the flow accelerates. This is because, as stated previously, the model for the effective viscosity assumes that the flow becomes fully turbulent beyond $y^+ = 26$, no matter what pressure gradient occurs.

Equation (11) gives a fair representation of the law of the wall region of the measured velocity profiles at stations 1 and 2 for the adiabatic case. This is to be expected because equation (11) is based on analysis of zero pressure gradient flows. At stations 3 and 4 no comparison is possible, but at station 5 both the adiabatic and the heat-transfer cases yielded velocity profiles with regions which equation (11) represented fairly well. Although this could not be expected for heat-transfer case, previous measurements (ref. 6) have indicated that the adiabatic boundary layer near a nozzle throat can be represented by a form of the law of the wall. The only statement that can be made about the temperature profiles of figure 11 in relation to equation (11) is that the relative slopes indicate that a definite law of the wall region exists at every station. The difference in

level between the measured data and equation (11) can be partly attributed to the assumption of unit Prandtl number implicit in the equation.

The velocity portion of equation (11) is also the basis for the cross plot technique (ref. 16) used to estimate the friction coefficients C_f corresponding to the present boundary layer measurements (figs. 8 and 9). Essentially, this method requires finding a region within the measured velocity profiles where the law of the wall is valid, or where the shear velocity, is constant. Knowing u_τ, from

$$u_\tau = u_e\left(\frac{T_w}{T_e}\right)^{1/2}\left(\frac{C_f}{2}\right)^{1/2} \tag{12}$$

the local wall friction coefficient can be determined. This method, of course, requires that the law of the wall (eq. (11)) be valid in the flow field to which it is applied, which is probably only strictly true in flat plate type flows. Therefore, difficulty in applying the cross-plot method to boundary layers with strong pressure gradients might be expected. In flows such as those examined here, where the law of the wall region becomes very small or disappears completely, the method is highly difficult to apply. Figure 8 indicates that the cross plot method of determining C_f and the prediction of reference 7 agreed fairly well, particularly when the measured velocity profile was used as the initial condition for integration of the boundary layer equations. Figure 9 shows that, for the heat transfer case, the two methods did not agree. Since the method of reference 7 accounts for pressure gradient effects, the C_f values calculated by it are considered more accurate. The agreement between the predicted and measured values of displacement and momentum thicknesses indicate this to be true. However, the actual and predicted values of friction coefficient are undoubtedly only close in regions where the boundary-layer acceleration is small enough to avoid laminarization. This has been referred to by the authors of reference 7 in connection with their attempt to predict the heat-transfer data of reference 3 and is attributed to the effective viscosity hypothesis containing laminar effects only very near to the wall.

It should be noted that both methods of predicting C_f yielded maximum values very close to the axial position where the acceleration parameter K was also a maximum. The predicted values of C_f in the region of maximum acceleration seem to be high when compared with calculated and measured friction coefficients in known turbulent flows (ref. 7). A definite possibility for this occurrence could be the reduction of turbulence level below that where the classical models of the turbulent boundary layer are valid, as suggested above in connection with reference 7. As stated previously, a laminarized or transition type boundary layer may have existed in the region where the acceleration parameter K reached its maximum value.

Another difficulty in applying the prediction method of reference 7 is indicated in figures 8 and 9. The calculated values of all parameters were strongly dependent on the initial condition in the upstream region, where the pressure gradient was small. Where the acceleration was large, the results are relatively insensitive to upstream history. When the measured velocity and temperature profiles at station 1 were used to initiate the integration, the calculated and predicted values of the boundary layer thicknesses agree reasonably well. The largest errors occurred where the acceleration, based on K, was high. At stations 2 and 5 (M_e = 0.24 and 0.97) the average error in displacement, momentum, and energy thicknesses was 8 percent. At station 3 (M_e = 0.42), where K was highest, and immediately downstream at station 4 (M_e = 0.54), the average error was 29 percent. Average error in the predicted values of δ and Δ was 15 percent at stations 2 and 5, and 26 percent at stations 3 and 4. However, due to the asymptotic nature of the boundary layer, errors would also be expected in the measured values of δ and Δ, making the predicted values less meaningful. The quantitative agreement between the measured and predicted profiles of figures 6 and 7 is more difficult to analyze, but undoubtedly the pressure gradient plays a large part in yielding the indicated differences.

Results of the attempted heat-transfer measurement are presented in the appendix. Calculated values of the heat-transfer parameters, using the method of reference 7, are also presented.

SUMMARY OF RESULTS

Experimental velocity and temperature profiles for the adiabatic and cooled boundary layers on a cylindrical body in an accelerated flow have been presented. The measurements were made over the Mach number range M_e = 0.21 to 0.97, and compared with a numerical integration of the boundary-layer equations using a standard mixing-length model for the turbulent viscosity. An attempt to measure the related heat transfer was not successful. The following results of the boundary-layer measurements and calculations were indicated:

1. A strong favorable pressure gradient caused the measured wake component of the velocity profile, normally associated with the turbulent boundary layer in zero and adverse pressure gradient flows, to disappear. The momentum layer was thinned by acceleration, but cooling the same boundary layer caused an increase in the velocity and momentum thicknesses over their corresponding adiabatic values. Acceleration effects were well correlated by the parameter $K = \left(\nu_e/u_e^2\right)\left/\left(du_e/dx\right)\right.$.

2. High acceleration caused the thermal boundary layer to become thicker than the momentum boundary layer. A noticeable wake component of the temperature profile

existed at each station. Increased resistance to heat transfer would undoubtedly result from the growth of the thermal boundary layer into a region of low eddy conductivity.

3. The extent of the boundary layer sublayer was difficult to evaluate because of its thinness and the lack of wall friction measurements. Thermal boundary-layer measurements, which must be qualified due to possible direct heat transfer between the probe and cold centerbody wall, indicate that high acceleration may have caused the sublayer to grow outside the bounds which characterize zero and adverse pressure gradient flows.

4. Standard models of the turbulent boundary layer yield friction coefficients in the region of highest acceleration larger than those normally measured or calculated. This is a possible indication of laminarization or a transition type boundary layer.

5. The numerical integration of the boundary-layer equations was strongly dependent on the initial condition where the pressure gradient was small, and almost independent where the pressure gradient was large. Predictions of momentum, displacement and energy thicknesses had an average error of 8 percent in regions of low acceleration, and 29 percent in regions of high acceleration.

Lewis Research Center,
National Aeronautics and Space Administration,
Cleveland, Ohio, July 30, 1970,
129-01.

APPENDIX - HEAT-TRANSFER MEASUREMENT

Use of the known heat storage capacity of a body to measure heat transfer has been used frequently (refs. 9 and 10). In its attempted application in this experiment, the measurement required the sudden removal of the coolant from the centerbody and monitoring the rate of wall temperature increase. Because of the high thermal conductivity of the copper wall and its thinness, a negligible temperature gradient existed in the radial direction. An energy balance on an element of the wall, shown in figure 12,

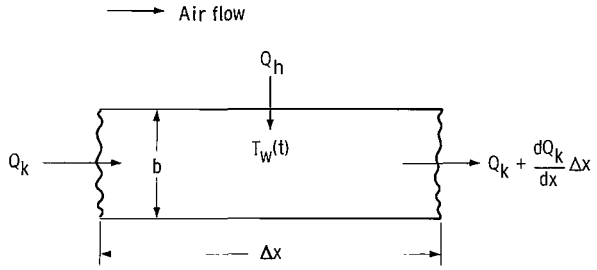

Figure 12. - Element of centerbody wall used in energy balance.

assuming no heat transfer to the coolant side, yields

Q_s (Rate of heat storage) = Q_h (Heat transfer from air) + Q_k (Heat conducted in at x)

$$- \left(Q_k + \frac{dQ_k}{dx}\Delta x\right) \quad \text{(Heat conducted out at } x + \Delta x) \tag{A1}$$

where

$$Q_s = \rho C_p b\, \Delta x \frac{dT_w}{dt} \tag{A2}$$

$$Q_k = -kb \frac{dT_w}{dx} \tag{A3}$$

$$Q_h = h\, \Delta x (T_{aw} - T_w) \tag{A4}$$

Unit thickness, perpendicular to the figure, is assumed in equations (A2) to (A4). Substitution of these relations in equation (A1) yields

$$h = \frac{b}{T_{aw} - T_w}\left[\rho C_p \frac{dT_w}{dt} - \frac{d}{dx}\left(k \frac{dT_w}{dx}\right)\right] \tag{A5}$$

Equation (A5) is correct at any time t after the coolant has been removed; however, it is only of practical interest at $t = 0$, the instant of the coolant's removal, when the heat transfer from the air is the same as during the steady state cooling period. By measuring the axial temperature gradient and the rate of temperature change at $t = 0$, it is then theoretically possible to determine the heat transfer coefficient at any axial position on the centerbody.

Practically, the measurement was not as straightforward as the theory indicates, since it is impossible to instantly remove the coolant from the centerbody. As explained in the APPARATUS section, the nitrogen coolant was removed from the centerbody by closing valves at the inlet and vent, and opening a valve to the vacuum system. This caused an expansion wave to propagate through the nitrogen remaining in the centerbody, which reduced the coolant temperature and, effectively, the wall temperature from its steady-state value. An example of the temperature history is given in figure 13, which shows the result of a measurement at $x = 0$. The time required to remove the nitrogen from the centerbody was estimated to be about 0.75 second by measuring the internal pressure of the centerbody with a transducer at its upstream end.

Measurement of the rate of temperature increase was with an automatic voltage

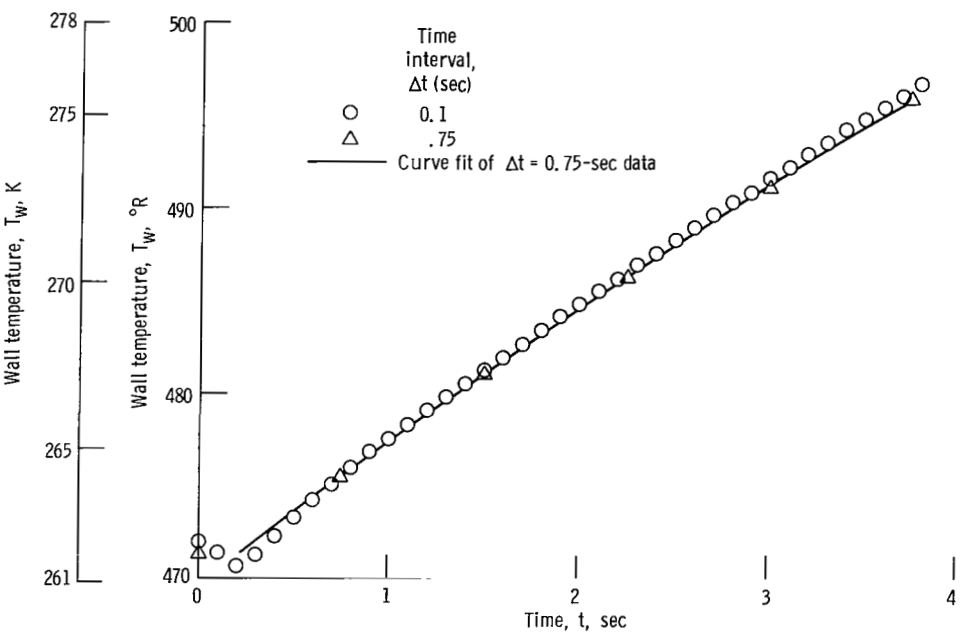

Figure 13. - Transient wall temperature at $x = 0$.

digitizer (AVD) system which read each thermocouple at 0.75-second intervals. Because of the finite purge time for the coolant, the data from t = 0 to 0.75 second, was ignored in the data reduction process. Although data were recorded for periods as long as 30 seconds, only those from t = 0.75 to 4.00 seconds were used for the curve fit necessary to determine dT_w/dt, so that the best possible accuracy could be attained near t = 0. The effective value for dT_w/dt at t = 0 was determined by using the curve fit to extrapolate back to the steady state temperature at each thermocouple station. Temperatures in the time direction were curve fit with a second order polynomial, using the least squares method. Accuracy of this method depended on the range of temperatures included in the time interval considered. The greatest difference between measured and curve fit temperature was about 0.3° R (0.54 K) at x = 10.531 inches (0.268 m), where the largest heat flux was measured. Accuracy of the extrapolation was checked by measuring each of four thermocouples separately with the AVD at 0.10 second intervals. Figure 13 shows a comparison of readings taken at 0.10 second intervals with those taken at 0.75-second intervals for the thermocouple at x = 0, along with the curve fit. Determinations of dT_w/dt, using the data measured at the two sampling rates, differed by no more than 5 percent.

The conduction term in equation (A5) was evaluated by assuming that over the narrow range of temperatures attained by the centerbody during steady-state conditions, k could be considered constant, resulting in

$$\frac{d}{dx}\left(k\frac{dT_w}{dx}\right) = k\frac{d^2T_w}{dx^2} \tag{A6}$$

For the measurement to be accurate, the heat conduction term must be small relative to the heat storage term in equation (A5), which is the case in all successful applications of this method. As shown in the RESULTS AND DISCUSSION section, the axial temperature distribution was not smooth and, in particular, a sharp peak existed near the nozzle throat. As a result, evaluation of the second derivative in the conduction term became a highly inaccurate process. In particular, wherever a peak existed in the axial temperature distribution, the magnitude of the conduction term varied over a wide range, depending on the order of the curve fit used to approximate the distribution. The most accurate approximations (highest order curve fits) resulted in values having the same order of magnitude as the heat storage term. Therefore, since evaluation of the second derivative of experimental data of the type presented here cannot be considered accurate, the heat-transfer measurement was invalidated.

Some results of the attempted heat transfer measurement are shown in figure 14. Stanton number and heat transfer coefficient distributions, as measured by the above method with $\left(d^2T_w/dx^2\right) = 0$, are indicated. The error band shown for the downstream

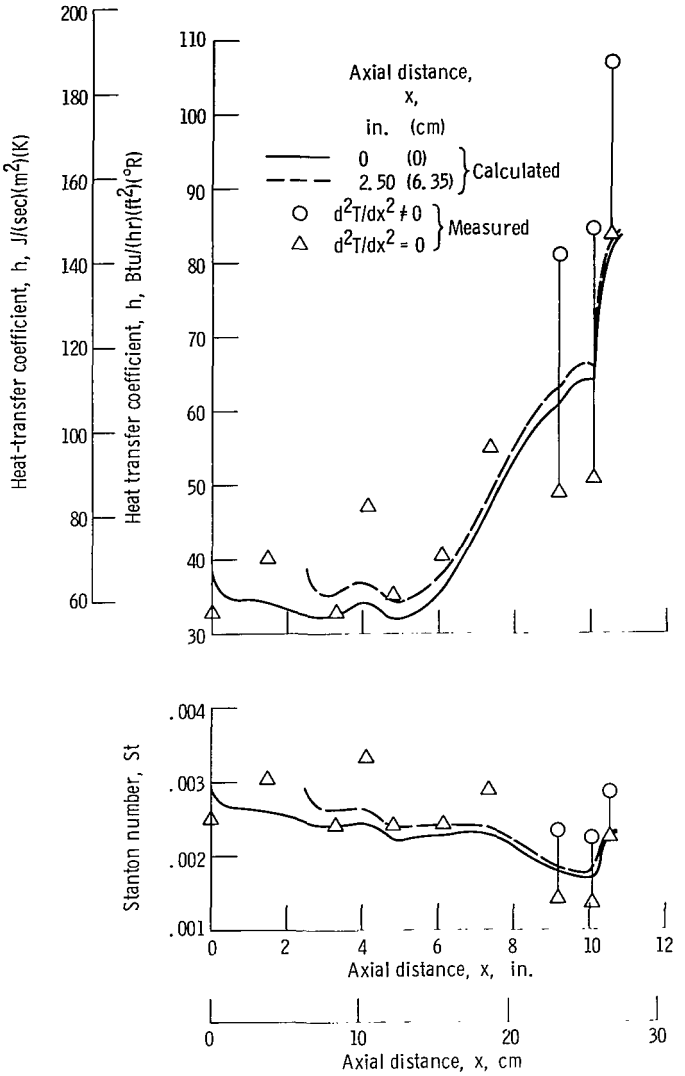

Figure 14. - Heat-transfer data and calculations from reference 7.

data points indicate the difference between neglecting the conduction term and using a second order least squares polynomial to approximate d^2T_w/dx^2 in this region. When a similar approximation was used in the upstream region, the error bands were negligible, and thus are not indicated. Also shown in figure 14 are results from the prediction method of reference 7, using the two initial conditions discussed in the RESULTS AND DISCUSSION section. The calculations indicate a significant decrease in Stanton number or heat transfer level, immediately downstream of the region of highest acceleration, which indicates a qualitative comprehension of pressure gradient effects by the prediction method.

Two difficulties are believed to have contributed to the failure of the heat transfer

measurement. The coolant flow passage was very cluttered due to the large number of instrument leads required to pass through the small diameter centerbody. However, because of problems in assembling such small instrumentation, no better design existed, and the result was an unsmooth temperature distribution. Also, as mentioned previously, a sharp peak existed in the temperature profile near the nozzle throat. This was due entirely to the strong favorable pressure gradient, and is typical of nozzle heat-transfer data where the nozzle convergence angle is steep. An experimental design incorporating a clear coolant flow passage, and avoiding the difficulties of measurement near a nozzle throat, could probably apply the transient heat transfer method successfully.

REFERENCES

1. Boldman, Donald R.; Schmidt, James F.; and Gallagher, Anne K.: Laminarization of a Turbulent Boundary Layer as Observed from Heat-Transfer and Boundary-Layer Measurements in Conical Nozzles. NASA TN D-4788, 1968.

2. Graham, Robert W.; and Boldman, Donald R.: The Use of Energy Thickness in Prediction of Throat Heat Transfer in Rocket Nozzles. NASA TN D-5356, 1969.

3. Moretti, P. M.; and Kays, W. M.: Heat Transfer Through an Incompressible Turbulent Boundary Layer with Varying Free-Stream Velocity and Varying Surface Temperature. Rep. PG-1, Thermosciences Div., Mech. Eng. Dept., Stanford Univ., Nov. 1964.

4. Kays, W. M.; Moffat, R. J.; and Thielbahr, W. H.: Heat Transfer to the Highly Accelerated Turbulent Boundary Layer With and Without Heat Transfer. Paper 69-HT-53, ASME, Aug. 1969.

5. Back, L. H.; Massier, P. F.; and Cuffel, R. F.: Some Observations on Reduction of Turbulent Boundary-Layer Heat Transfer in Nozzles. AIAA J., vol. 4, no. 12, Dec. 1966, pp. 2226-2229.

6. Wesoky, Howard L.: Boundary-Layer Measurements in Accelerated Flows Near Mach 1. NASA TN D-3882, 1967.

7. Patankar, S. V.; and Spalding, D. B.: Heat and Mass Transfer in Boundary Layers. C. R. C. Press, 1968.

8. Gettelman, Clarence C.; and Krause, Lloyd N.: Considerations Entering into the Selection of Probes for Pressure Measurement in Jet Engines. ISA Proceedings, 1952, Paper No. 52-12-1.

9. Thomann, H.; and Lindsjoe, G.: Optimization of the Reduction of Transient Heat Transfer Data. Rep. FFA-106, Aeronautical Research Institute of Sweden, Mar. 1966.

10. Wilson, Donald M.; and Fisher, Paul D.: Effect of a Highly Cooled Wall on Hypersonic Turbulent Heat Transfer. Rep. NOLTR-65-153, Naval Ordnance Lab., June 1, 1966. (Available from DDC as AD-638232.)

11. Ames Research Staff: Equations, Tables, and Charts for Compressible Flow. NACA TR 1135, 1953.

12. Schubauer, G. B.; and Tchen, C. M.: Turbulent Flow. Turbulent Flows and Heat Transfer. Vol. 5 of High Speed Aerodynamics and Jet Propulsion. C. C. Lin, ed., Princeton Univ. Press, 1959.

13. Coles, D. E.; and Hirst, E. A.: Computation of Turbulent Boundary Layers. 1968 AFOSR-IFP-Stanford Conference. Vol. II. Thermosciences Div., Mech. Eng. Dept., Stanford Univ., 1969.

14. Quarmby, Alan; and Das, H. K.: Displacement Effects on Pitot Tubes with Rectangular Mouths. Aeron. Quart., vol. 20, May 1969, pp. 129-139.

15. Galezowski, Stanley H.: Effects of Probe Tip Geometry and Size on Measurements in a Laminar Boundary Layer in Supersonic Flow. Tech. Note 17, Inst. of Aerophysics, Univ. Toronto, Oct. 1957.

16. Clauser, F. H.: Turbulent Boundary Layers in Adverse Pressure Gradients. J. Aeronaut. Sci., vol. 21, Feb. 1954, pp. 91-108.

NASA-Langley, 1970 —— 12 E-5674

"The aeronautical and space activities of the United States shall be conducted so as to contribute . . . to the expansion of human knowledge of phenomena in the atmosphere and space. The Administration shall provide for the widest practicable and appropriate dissemination of information concerning its activities and the results thereof."

—NATIONAL AERONAUTICS AND SPACE ACT OF 1958

NASA SCIENTIFIC AND TECHNICAL PUBLICATIONS

TECHNICAL REPORTS: Scientific and technical information considered important, complete, and a lasting contribution to existing knowledge.

TECHNICAL NOTES: Information less broad in scope but nevertheless of importance as a contribution to existing knowledge.

TECHNICAL MEMORANDUMS: Information receiving limited distribution because of preliminary data, security classification, or other reasons.

CONTRACTOR REPORTS: Scientific and technical information generated under a NASA contract or grant and considered an important contribution to existing knowledge.

TECHNICAL TRANSLATIONS: Information published in a foreign language considered to merit NASA distribution in English.

SPECIAL PUBLICATIONS: Information derived from or of value to NASA activities. Publications include conference proceedings, monographs, data compilations, handbooks, sourcebooks, and special bibliographies.

TECHNOLOGY UTILIZATION PUBLICATIONS: Information on technology used by NASA that may be of particular interest in commercial and other non-aerospace applications. Publications include Tech Briefs, Technology Utilization Reports and Technology Surveys.

Details on the availability of these publications may be obtained from:

SCIENTIFIC AND TECHNICAL INFORMATION OFFICE

NATIONAL AERONAUTICS AND SPACE ADMINISTRATION

Washington, D.C. 20546